Nuclear Reactions

Yukawa potential: $$V(r) = \frac{g\hbar c}{r}\exp(-r/r_0) .$$

This potential has two limits:

$r_0 \to \infty$ and $r_0 \to 0$. In the first limit the Yukawa potential becomes the Coulomb potential

$$V(r) = \frac{g\hbar c}{r} \qquad g = Z_1 Z_2 \alpha ,$$

where Z_1 and Z_2 are the charges of the interacting particles and $\alpha = e^2/4\pi\epsilon_0\hbar c \sim 1/137$ is the fine structure constant. In the other limit $r_0 \to 0$, the potential is

$$V(r) = 4\pi G\delta^3(\boldsymbol{r}) \qquad G = g\hbar c r_0^2 .$$

This potential is useful in discussing weak-interaction processes where G is of order the Fermi constant G_{F}. The techniques of Sect. 3.2 will therefore allow us to treat scattering and reactions due to the weak and electromagnetic interactions.

Section 3.4 will show how to take into account the fact that the scattering potential is not fixed, but due to a particle that will itself recoil from the collision. This will allow us to treat processes where the target is a complicated collection of particles that can be perturbed by the beam particle. With these techniques, we will learn how it is possible to determine the charge distribution in nuclei.

Section 3.5 will show how short-lived "resonances" can be produced during collisions.

Section 3.6 will introduce the more difficult problem of nucleon–nucleon and nucleon–nucleus scattering where the interaction potential can no longer be considered as weak. This problem will complete our treatment of the deuteron in Sect. 1.4.

Finally, in Sect. 3.7 we will learn how coherent forward scattering in a medium leads to a neutron refractive index. An application of this subject will be the production of ultra low-energy neutron beams.

To introduce cross-sections, it is conceptually simplest to consider a thin slice of matter of area L^2 containing N spheres of radius R, as shown in Fig. 3.1. A point-like particle impinging upon the slice at a random position will have

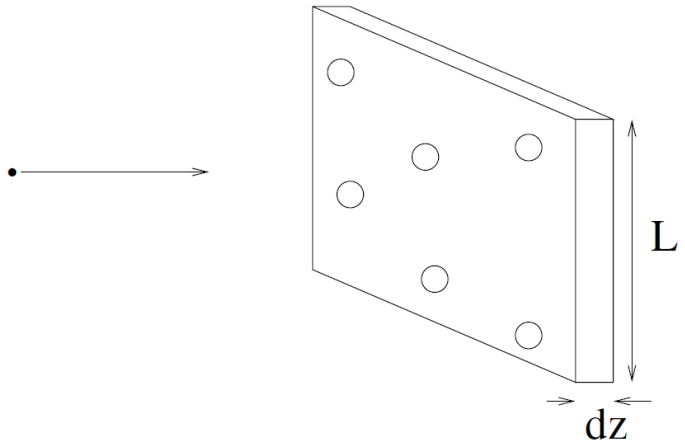

Fig. 3.1. A small particle incident on a slice of matter containing $N = 6$ target spheres of radius R. If the point of impact on the slice is random, the probability $\mathrm{d}P$ of it hitting a target particle is $\mathrm{d}P = N\pi R^2/L^2 = \sigma n \mathrm{d}z$ where the number density of scatterers is $n = N/(L^2\mathrm{d}z)$ and the cross section per sphere is $\sigma = \pi R^2$.

a probability $\mathrm{d}P$ of hitting one of the spheres that is equal to the fraction of the surface area covered by a sphere

$$\mathrm{d}P \;=\; \frac{N\pi R^2}{L^2} \;=\; \sigma n \mathrm{d}z \qquad\qquad \sigma \;=\; \pi R^2 \;. \tag{3.4}$$

In the second form, we have multiplied and divided by the slice thickness $\mathrm{d}z$ and introduced the number density of spheres $n = N/(L^2\mathrm{d}z)$. The "cross-section" for touching a sphere, $\sigma = \pi R^2$, has dimensions of "area/sphere."

While the cross-section was introduced here as a classical area, it can be used to define a probability $\mathrm{d}P_\mathrm{r}$ for any type of reaction, r, as long as the probability is proportional to the number density of target particles and to the target thickness:

$$\mathrm{d}P_\mathrm{r} \;=\; \sigma_\mathrm{r}\, n\, \mathrm{d}z \;. \tag{3.5}$$

The constant of proportionality σ_r clearly has the dimension of area/particle and is called the cross-section for the reaction r.

If the material contains different types of objects i of number density and cross-section n_i and σ_i, then the probability to interact is just the sum of the probabilities on each type:

$$\mathrm{d}P \;=\; \sum_i n_i \sigma_i \tag{3.6}$$

Because nuclear radii are of order of a few femtometer we can anticipate that the cross-sections for nuclear reactions involving the strong interactions will often be of order $1\,\mathrm{fm}^2$. In fact, the units of cross-section most often used is the "barn,"

$$1\,\mathrm{b} = 100\,\mathrm{fm}^2 = 10^{-28}\,\mathrm{m}^2 \,. \tag{3.7}$$

We will see in this chapter that nuclear weak interactions generally have cross-sections about 20 orders of magnitude smaller.

It should be emphasized that (3.5) supposes that the total probability for a type of reaction is found by summing the probabilities for reactions on each particle in the target. This assumption breaks down if interference is important, as in Bragg scattering on crystals or in elastic scattering at very small angles. In these cases, it is necessary to add *amplitudes* for scattering on target particles rather than *probabilities*. We emphasize that, in fact, adding amplitudes *always* gives the correct probability but in most cases the random phases for amplitudes from different target particles gives a $\mathrm{d}P$ that is proportional to the number of scatters rather than to its square. Equation (3.5) is therefore applicable except in special circumstances.

While we have introduced the cross-section in the context of particles incident upon a target, cross-sections are of more general applicability. For example, consider a pulse of classical electromagnetic radiation of a given energy density that impinges on a target. A cross-section can then be defined in terms of the fraction $\mathrm{d}F$ of *energy flux* that is scattered out of the original direction

$$\mathrm{d}F = \sigma n \mathrm{d}z \,. \tag{3.8}$$

We can take n to be the number density of atoms, so σ has dimensions of area/atom. This definition of the cross-section makes no reference to incident particles but only to incident energy.

The Thomson scattering cross-section of photons on electrons was originally derived in this manner by treating the interaction between a classical electromagnetic wave and free electrons. Consider a plane wave propagating in the z direction with the electric field oriented along the x direction:

$$E_x = E\cos(kz - \omega t) \,. \tag{3.9}$$

The (time averaged) electromagnetic energy energy flux (energy per unit area per unit time) is proportional to the square of the electric field:

$$\text{incident energy flux} = \frac{\epsilon_0 c E^2}{2} \,. \tag{3.10}$$

Suppose there is a free electron placed at the origin. It will be accelerated by the electric field and will oscillate in the direction of the electric field with its acceleration given by

$$\ddot{x}(t) \;=\; \frac{eE}{m_{\mathrm{e}}}\cos(\omega t)\;. \tag{3.11}$$

The accelerated charge then radiates electromagnetic energy with a power given by the Larmor formula:

$$\text{radiated power} \;=\; \frac{e^2}{6\pi\epsilon_0 c^3}\langle\ddot{x}^2\rangle \;=\; c\frac{4\pi}{3}\epsilon_0 E^2\left(\frac{e^2}{4\pi\epsilon_0 m_{\mathrm{e}}c^2}\right)^2\;, \tag{3.12}$$

where $\langle\rangle$ means time-average. The total cross-section defined by (3.8) is

$$\sigma \;=\; \frac{\text{power radiated}}{\text{incident energy flux}} \;=\; \frac{8\pi}{3}\left(\frac{e^2}{4\pi\epsilon_0 m_{\mathrm{e}}c^2}\right)^2 \;=\; 0.665\,\mathrm{b}\;. \tag{3.13}$$

This is just the famous Thomson cross-section for the scattering of an electromagnetic wave on a free electron. Quantum mechanically, this can be interpreted as the scattering of photons on free electrons. Since the energy flux is proportional to the photon flux, the Thomson cross-section is the cross-section for the elastic scattering of photons on electrons. It turns out that the quantum-mechanical calculation gives the same result in the limit $\hbar\omega \ll m_{\mathrm{e}}c^2$, i.e. that the photon energy be much less than the electron rest energy. The cross-section for higher energy photons and for photons scattering on bound electrons requires a quantum-mechanical calculation.

Differential cross-sections

The probability for elastic scattering is determined by the elastic scattering cross-section

$$\mathrm{d}P_{\mathrm{el}} \;=\; \sigma_{\mathrm{el}}\, n\,\mathrm{d}z\;. \tag{3.14}$$

Going beyond this simple probability, we can ask what is the probability that the elastic scatter results in the particle passing through a detector of area $\mathrm{d}x^2$ at a distance r from the target and angle θ with respect to the initial direction. The geometry in shown in Fig. 3.2 where the detector is oriented so that it is perpendicular to the vector between it and the target.

The probability is proportional to the product of the probability of a scatter and the probability that the scattered particle goes through the detector. If the scattering angle is completely random, the second is just the ratio of $\mathrm{d}x^2$ and the area of the sphere surrounding the target

$$\mathrm{d}P_{\mathrm{el},\theta} \;=\; \sigma_{\mathrm{el}}\, n\, \mathrm{d}z \frac{\mathrm{d}x^2}{4\pi r^2} \qquad \text{isotropic scattering .} \tag{3.15}$$

The solid angle covered by the detector is $\mathrm{d}\Omega = \mathrm{d}x^2/r^2$ so

$$\mathrm{d}P_{\mathrm{el},\theta} \;=\; \frac{\mathrm{d}\sigma}{\mathrm{d}\Omega}\, n\, \mathrm{d}z\, \mathrm{d}\Omega \;, \tag{3.16}$$

where the differential scattering cross section is $\mathrm{d}\sigma/\mathrm{d}\Omega = \sigma_{\mathrm{el}}/4\pi$ for isotropic scattering. In general, the scattering is not isotropic so $\mathrm{d}\sigma/\mathrm{d}\Omega$ is a function of θ. If the target or beam particles are polarized, it can be a function of the azimuthal angle ϕ.

The total elastic cross-section determines the total probability for elastic scattering so

$$\sigma_{\mathrm{el}} \;=\; \int \mathrm{d}\Omega \frac{\mathrm{d}\sigma}{\mathrm{d}\Omega} \;=\; \int_0^{2\pi} \mathrm{d}\phi \int_0^{\pi} \sin\theta \mathrm{d}\theta \frac{\mathrm{d}\sigma}{\mathrm{d}\Omega}(\theta,\phi) \;. \tag{3.17}$$

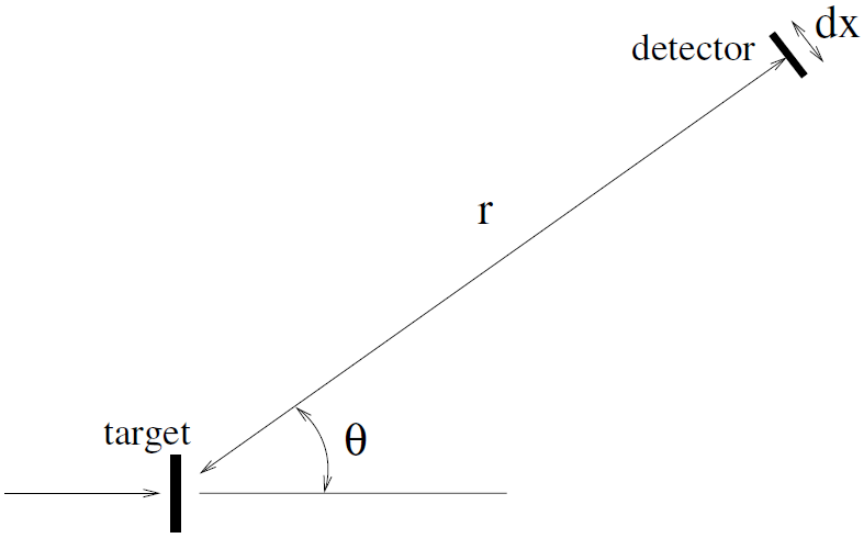

Fig. 3.2. A particle incident on a thin slice of matter containing n scatterers per unit volume of cross-section σ. A detector of area $\mathrm{d}x^2$ is placed a distance r from the target and oriented perpendicular to $\boldsymbol{r}$. If an elastic scatter results in a random scattering angle, the probability to detect the particle is $\mathrm{d}P = n\mathrm{d}z\sigma(\mathrm{d}x^2/4\pi r^2) = n\mathrm{d}z(\sigma/4\pi)\mathrm{d}\Omega$, where $\mathrm{d}\Omega = x^2/r^2$ is the solid angle covered by the detector.

Inelastic and total cross-sections

In general for a reaction creating N particles

$$a\; b \rightarrow\; x_1\; x_2 \ldots x_N \tag{3.18}$$

the probability to create the particles x_i in the momentum ranges $\mathrm{d}^3\boldsymbol{p}_i$ centered on the momenta $\boldsymbol{p}_i$ is given by

$$\mathrm{d}P \;=\; \frac{\mathrm{d}\sigma}{\mathrm{d}^3\boldsymbol{p}_1 \ldots \mathrm{d}^3\boldsymbol{p}_N}\, n_b\, \mathrm{d}z\, \mathrm{d}^3\boldsymbol{p}_1 \ldots \mathrm{d}^3\boldsymbol{p}_N \;. \tag{3.19}$$

The differential cross-section $\mathrm{d}\sigma/\mathrm{d}^3\boldsymbol{p}_1 \ldots \mathrm{d}^3\boldsymbol{p}_N$ will be a singular function because only energy–momentum conserving combinations have non-vanishing probabilities.

The total probability for the reaction $a\,b \to x_1 \ldots x_N$ is

$$\mathrm{d}P_{ab\to x_1 \ldots x_N} \;=\; \sigma_{ab\to x_1 \ldots x_N} n_b \mathrm{d}z \tag{3.20}$$

where the reaction cross-section is

$$\sigma_{ab\to x_1 \ldots x_N} \;=\; \int \mathrm{d}^3\boldsymbol{p}_1 \ldots \int \mathrm{d}^3\boldsymbol{p}_N \frac{\mathrm{d}\sigma}{\mathrm{d}^3\boldsymbol{p}_1 \ldots \mathrm{d}^3\boldsymbol{p}_N} \mathrm{d}^3\boldsymbol{p}_1 \ldots \mathrm{d}^3\boldsymbol{p}_N \;. \tag{3.21}$$

The total probability that "anything" happens to the incident particle as it traverses the target of thickness $\mathrm{d}z$ is just the sum of the probabilities of the individual reactions

$$\mathrm{d}P \;=\; \sigma_{\mathrm{tot}} n_b \mathrm{d}z \tag{3.22}$$

where the total cross-section is

$$\sigma_{\mathrm{tot}} \;=\; \sum_i \sigma_i \;. \tag{3.23}$$

The uses of cross-sections

Cross-sections enter into an enormous number of calculations in physics. Consider a thin target (Fig. 3.1) containing a density n of target particles that is subjected to a flux of beam particles F (particles per unit area per unit time). If particles that interact in the target are considered to be removed from the beam (scattered out of the beam or changed into other types of particles), then the probability for interaction $\mathrm{d}P = \sigma n_{\mathrm{b}} \mathrm{d}z$ implies that the F is reduced by

$$\mathrm{d}F \;=\; -F\sigma n \mathrm{d}z \;, \tag{3.24}$$

equivalent to the differential equation

$$\frac{\mathrm{d}F}{\mathrm{d}z} \;=\; -\frac{F}{l} \;, \tag{3.25}$$

where the "mean free path" l is

$$l \;=\; \frac{1}{n\sigma} \;. \tag{3.26}$$

For a thick target, (3.25) implies that the flux declines exponentially

$$F(z) \;=\; F(0)\mathrm{e}^{-z/l}\;. \tag{3.27}$$

If the material contains different types of objects i of number density and cross-section n_i and σ_i, then (3.6) implies that the mean free path is given by

$$l^{-1} \;=\; \sum_i n_i\sigma_i\;. \tag{3.28}$$

The mean lifetime of a particle in the beam is the mean free path divided by the beam velocity v

$$\tau \;=\; \frac{l}{v} \;=\; \frac{1}{n_{\mathrm{T}}\sigma_{\mathrm{tot}}v}\;. \tag{3.29}$$

The inverse of the mean lifetime is the "reaction rate"

$$\lambda \;=\; n\sigma_{\mathrm{tot}}v\;. \tag{3.30}$$

We will see that quantum-mechanical calculations most naturally yield the reaction rate from which one can derive the cross-section by dividing by nv.

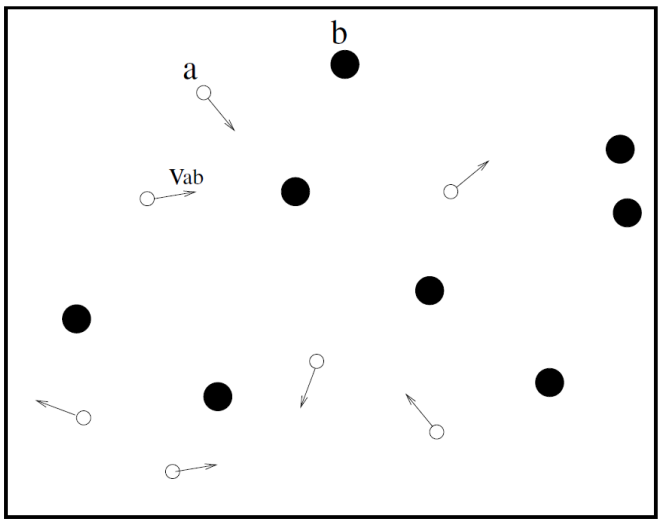

Fig. 3.3. A box containing two types of particles, a and b. The a particles move in random directions with velocity v_{ab} and can interact with the b particles (at rest) to form particles c and d with cross-section $\sigma_{ab\to cd}$. The time rate of change of the number density of particles a is determined by the Boltzmann equation (3.31).

The reaction rate enters directly into the "Boltzmann equation" governing the number density n_a of particles of type a confined to a region of space that contains particles of type b (Fig. 3.3). If the a particles are destroyed by the reaction $a\,b \to c\,d$, we have

$$\frac{\mathrm{d}n_a}{\mathrm{d}t} \;=\; -\frac{n_a}{\tau} \;=\; -n_a n_b\,\sigma_{ab\to cd}v_{ab}\;, \tag{3.31}$$

where v_{ab} is the relative velocity. (Of course it will be necessary to average the cross-section times velocity over the spectrum of particles.) The solution is just $n_a(t) = n_a(0)\exp(-t/\tau)$ as expected from (3.29).

If the region also contains particles of types c and d, particles of type a can also be created by the inverse reaction so the full Boltzmann equation is

$$\frac{\mathrm{d}n_a}{\mathrm{d}t} = -n_a n_b \sigma_{ab\to cd} v_{ab} + n_c n_d \sigma_{cd\to ab} v_{cd} \,. \tag{3.32}$$

General characteristics of cross-sections

The magnitude of a reaction cross-section depends on the energetics of the reaction (elastic, inelastic–endothermic, inelastic–exothermic) and the interaction responsible for the reaction (strong, electromagnetic, or weak). Additionally, at low energy, inelastic reactions between positively charged ions are strongly suppressed by the Coulomb barrier. In this section we review how these effects are manifested in the energy (Fig. 3.4) and angular dependences (Fig. 3.6) of cross-sections.

Elastic scattering The elastic cross-section depends on whether or not the scattering is due to long-range Coulomb interactions or to short-range strong interactions. As we will see in Sect. 3.2, the differential cross-section between two isolated charged particles diverges at small angles like $\mathrm{d}\sigma/\mathrm{d}\Omega \propto \theta^{-4}$. The total elastic cross-section is therefore infinite. For practical purposes, this divergence is eliminated because the Coulomb potential is "screened" at large distances by oppositely charged particles in the target. Nevertheless, the concept of total elastic cross-section for charged particles is not very useful.

Elastic neutron scattering is due to the short-range strong interaction so the differential cross-section does not diverge at small angles and the total elastic cross-section (calculated quantum mechanically) is finite. The elastic cross-sections are shown in Fig. 3.4 for neutron scattering on ^{1}H, ^{2}H and ^{6}Li. The ^{1}H cross-section is flat at low energy before decreasing slowly for $E > 1\,\mathrm{MeV}$. The low energy value, $\sigma_{\mathrm{el}} \sim 20\,\mathrm{b}$, is surprisingly large compared to that expected from the range of the strong interaction, $\pi(2\,\mathrm{fm})^2 \sim 0.1\,\mathrm{b}$. We will see in Sect. 3.6 that this is due to the fact that the proton–neutron system is slightly unbound if the two spins are anti-aligned (and slightly bound if they are aligned). For neutron momenta greater than the inverse range r of the strong interactions, $p > \hbar/r$ [$p^2/2m_{\mathrm{n}} > \hbar^2/(r^2 m_{\mathrm{n}}) > 1\,\mathrm{MeV}$], the cross-section drops down to a value more in line with the value expected from the range of the strong interactions.

The elastic cross-section for ^{6}Li shows a resonance at $E_n \sim 200$ keV which results from the production of an excited state of ^{7}Li that decays back to n ^{6}Li. The level diagram of ^{7}Li is shown in Fig. 3.5. For heavy nuclei, there are many excited states leading to a very complicated energy dependence of the cross-section, as illustrated for uranium in Fig. 3.26. The process of resonant production will be discussed in Sect. 3.5.

The angular distribution for elastic neutron–nucleus scattering is isotropic as long as $p < \hbar/R$ (R=nuclear radius) as illustrated in Fig. 3.6 and explained in Sect. 3.6. For $p > \hbar/R$ the angular distribution approaches that expected for diffraction from a semi-opaque object of radius R.

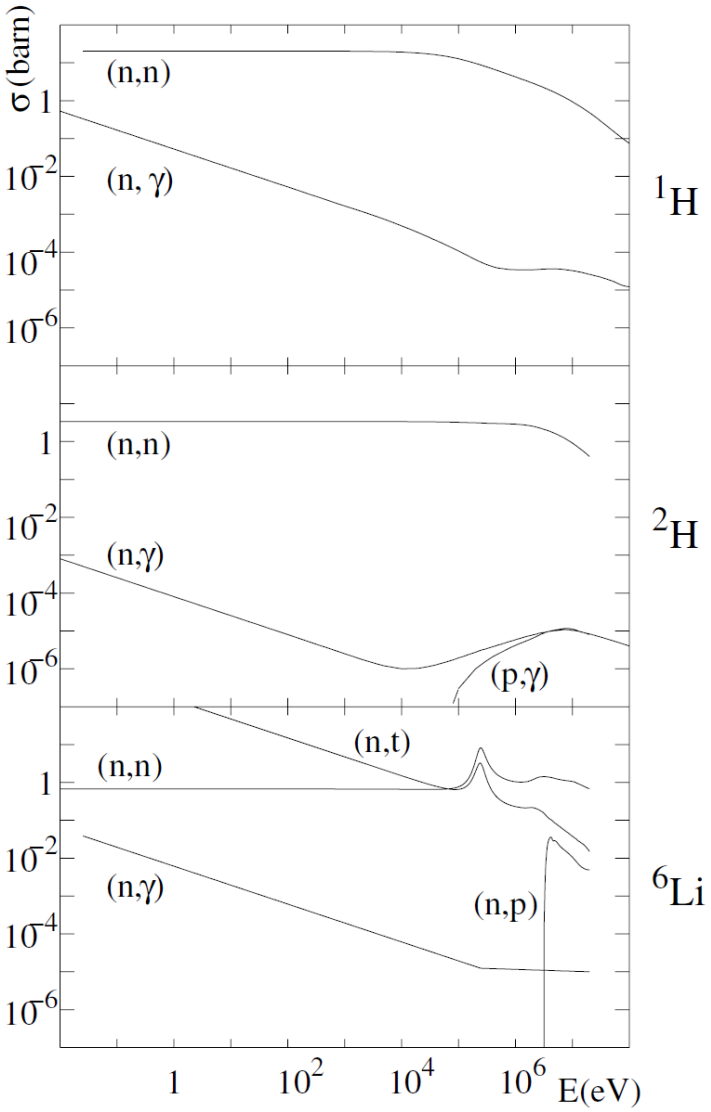

Fig. 3.4. Examples of reaction cross-sections on ^{1}H, ^{2}H, and ^{6}Li [30]. Neutron elastic scattering, (n,n), has a relatively gentle energy dependence while the exothermic reactions, (n, γ) and ^{6}Li(n, t)^{4}He (t=tritium=^{3}H), have a $1/v$ dependence at low energy. The exothermic (p, γ) reaction is suppressed at low energy because of the Coulomb barrier. The reaction ^{6}Li(n, p)^{6}Be has an energy threshold. The fourth excited state of ^{7}Li (Fig. 3.5) appears as a prominent resonance in n^{6}Li elastic scattering and in ^{6}Li(n, t)^{4}He.

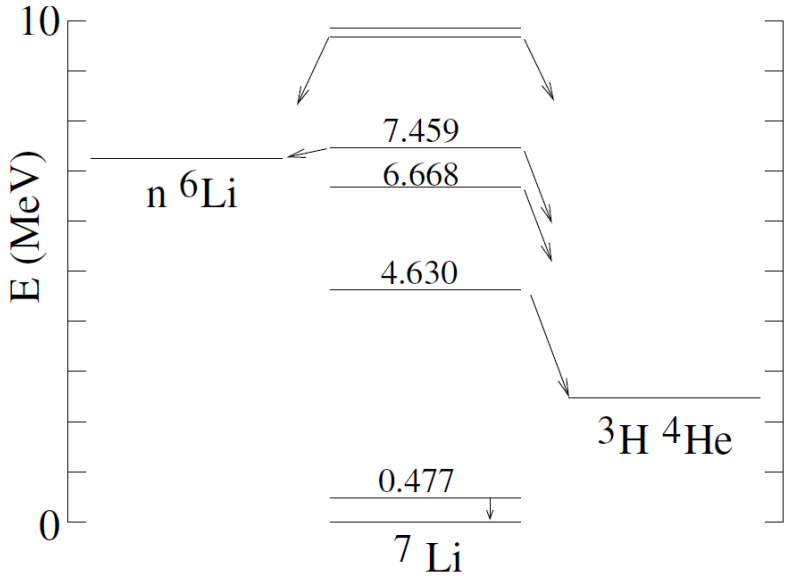

Fig. 3.5. The energy levels of ^{7}Li and two dissociated states n $-^6$ Li and ^{3}H $-$ ^{4}He. The first excited state of ^{6}Li decays to the ground state via photon emission while the higher excited states decay to ^{3}H$-^4$He. The fourth and higher excited states can also decay to n $-^6$ Li. The fourth excited state (7.459 MeV) appears prominently as a resonance in n ^{6}Li elastic scattering and in the exothermic (n,t) reaction n ^{6}Li $\rightarrow$ ^{3}H^{4}He. The resonance is seen at $E_{\rm n} \sim 200$ keV in Fig. 3.4.

Inelastic scattering Inelastic reactions with no Coulomb barrier have cross-section dependences at low energy that depend on whether the reaction is exothermic or endothermic. Exothermic reactions generally have cross-section proportional to the inverse of the relative velocity, $\sigma \propto 1/v$. This leads to a velocity-independent reaction rate $\lambda \propto \sigma v$. Examples in the figures are neutron radiative capture (n,γ) reactions. The nucleus ^{7}Li also has an exothermic strong reaction n^{7}Li $\rightarrow$ ^{3}H ^{4}He. The resonance observed in elastic scattering is also observed in the inelastic channel since the resonant state (Fig. 3.5) can decay to ^{3}H ^{4}He.

Endothermic reactions have an energy threshold as illustrated in Fig. 3.4 by the (n,p) reaction n^{6}Li $\rightarrow$ p^{6}Be.

Coulomb barriers The low-energy cross-section for inelastic reactions are strongly affected by Coulomb barriers through which a particle must tunnel for the reaction to take place. Cross-sections for two exothermic reactions on ^{2}H are shown in Fig. 3.4. The barrier-free (n,γ) reaction n ^{2}H $\rightarrow \gamma\,^3$H has the characteristic $1/v$ behavior at low energy. On the other hand, the (p,γ) reaction between charged particles p ^{2}H $\rightarrow \gamma\,^3$He is strongly suppressed at low energy. Its cross section becomes comparable to the (n,γ) reaction only for proton energies greater than the potential energy at the surface of the ^{6}Li nucleus $\sim 3\alpha\hbar c/2.4\,\mathrm{fm} \sim 1.8$ MeV.

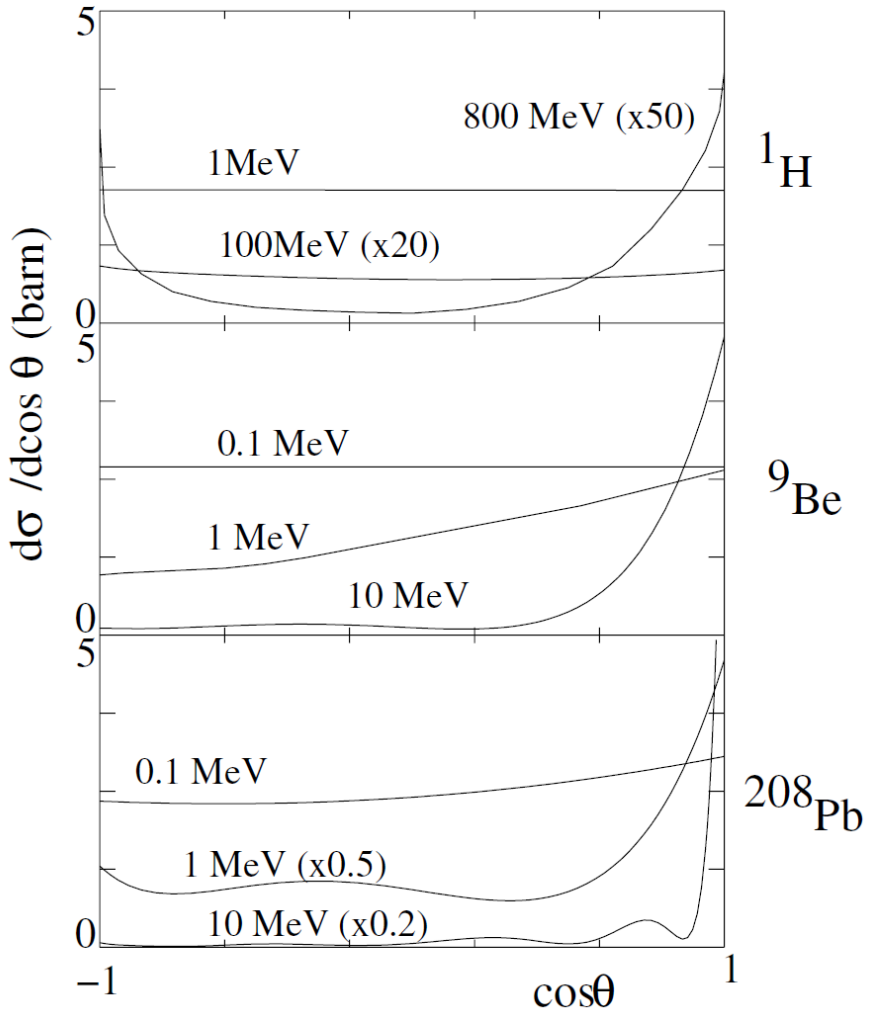

Fig. 3.6. The differential cross-section, $\mathrm{d}\sigma/\mathrm{d}\cos\theta = 2\pi\mathrm{d}\sigma/\mathrm{d}\Omega$, for elastic scattering of neutrons on ^{1}H, ^{9}Be and ^{208}Pb at incident neutron energies as indicated [30]. At low incident momenta, $p < \hbar/R_{\mathrm{nucleus}}$, the scattering is isotropic whereas for high momenta, the angular distribution resembles that of diffraction from a disk of radius R. Neutron scattering on ^{1}H at high-energy also has a peak in the backward directions coming from the exchange of charged pions (Fig. 1.13).

High-energy inelastic collisions The Coulomb barrier becomes ineffective at sufficiently high energy, $E_{\mathrm{cm}} > Z_1 Z_2 \alpha\hbar c/R$ where R is the sum of the radii of the nuclei of charges Z_1 and Z_2. In this case, the total inelastic cross-section becomes of order of the geometrical cross-section πR^2. At energies $< 1\,\mathrm{GeV}$, most inelastic collisions involve a simple break up of one or both of the nuclei, leading to the production of the unstable nuclei present in Fig. 0.2. These are called *fragmentation* reactions for medium-A nuclei while the breakup of a heavy nucleus is called *collision-induced fission*. Fragmentation of a target by protons or neutrons is called *spallation*.

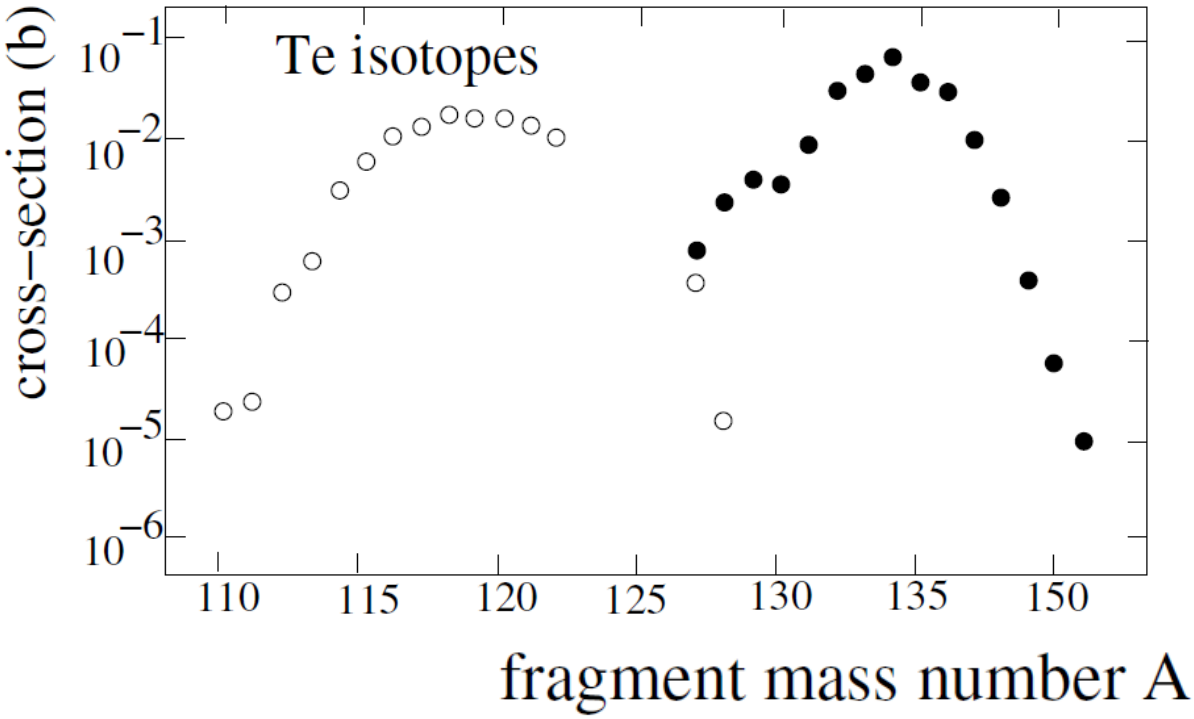

Fig. 3.7. The production of tellurium isotopes in the fragmentation of ^{129}Xe (790 MeV/nucleon) on a ^{27}Al target (open circles) and the collision-induced fission of ^{238}U (750 MeV/nucleon) on a Pb target (filled circles) [31]. Fragmentation leads to proton-rich isotopes while fission leads to neutron-rich isotopes.

Figure 3.7 gives the distribution of tellurium isotopes produced in the fragmentation of ^{129}Xe on a ^{27}Al target and the collision-induced fission of ^{238}U on a Pb target (filled circles) [31]. Fragmentation of Xe leads to proton-rich isotopes since mostly neutrons are ejected during the collision. Fission of uranium gives neutron-rich isotopes because of its large neutron-to-proton ratio. Reactions like these are the primary source of radioactive nuclides now used in the production of radioactive beams.

Occasionally, the target and projectile nuclei may fuse to form a much heavier nucleus. The produced nucleus is generally sufficiently excited to emit neutrons until a bound nucleus is produced. Such reactions are called *fusion–evaporation* reactions. This is the mechanism used to produce trans-uranium nuclei, as discussed in Sect. 2.8. The cross-section for the production of the heaviest elements is tiny, of order 10 pb for element 110.

For center-of-mass energies > 1 GeV/nucleon, inelastic nuclear collisions generally result in the production of pions and other hadrons. Collisions of cosmic-ray protons with nuclei in the upper atmosphere produce pions whose decays give rise to the muons that are the primary component of cosmic rays at the Earth's surface (Fig. 5.4).

Finally, we mention that for center-of-mass energies $> 100\,\mathrm{GeV/nucleon}$, certain collisions between heavy ions are believed to produce a state of matter called a *quark–gluon plasma* where the constituents of nucleons and hadrons are essentially free for a short time before recombining to form hadrons and nucleons. Such a state is also believed to exist in neutron stars (Sect. 8.1.2) and in the early Universe (Chap. 9).

Photons We have already calculated the cross-section (3.13) for elastic scattering of low-energy photons on free electrons. Since the cross-section is inversely proportional to the square of the electron mass, we can anticipate that the cross-section on free protons is 2000^2 times smaller and therefore negligible. This is because photon scattering is analogous to classical radiation of an accelerated charge, and a heavy proton is less easily accelerated than an electron.

The most important contributions to the photon cross-section on matter have nothing to do with nuclear physics. The important processes, shown in Fig. 5.12, are Compton scattering on atomic electrons

$$\gamma\,\mathrm{atom} \;\rightarrow\; \mathrm{atom}^{+}\,\mathrm{e}^{-}\,\gamma\,, \tag{3.33}$$

photoelectric absorption

$$\gamma\,\mathrm{atom} \;\rightarrow\; \mathrm{atom}^{+}\,\mathrm{e}^{-}\,, \tag{3.34}$$

and pair production

$$\gamma(A,Z) \;\rightarrow\; \mathrm{e}^{+}\mathrm{e}^{-}\,(\mathrm{A},\mathrm{Z})\,. \tag{3.35}$$

Pair production dominates at energies above the threshold $E_\gamma = 2m_\mathrm{e}c^2$.

Just as photons can breakup atoms through photoelectric absorption, they can excite or break up nuclei through photo-nuclear absorption. The cross-sections for this process on ^{2}H and ^{208}Pb are shown in Fig. 3.8. The cross-section for dissociation of ^{2}H exhibits a threshold at $E_\gamma = 2.22\,\mathrm{MeV}$, the binding energy of ^{2}H. The cross-section for dissociation of ^{208}Pb exhibits a broad *giant resonance* structure typical of heavy nuclei. Such resonances can be viewed semi-classically as the excitation of a *collective* oscillation of the proton in the nucleus with respect to the neutrons.

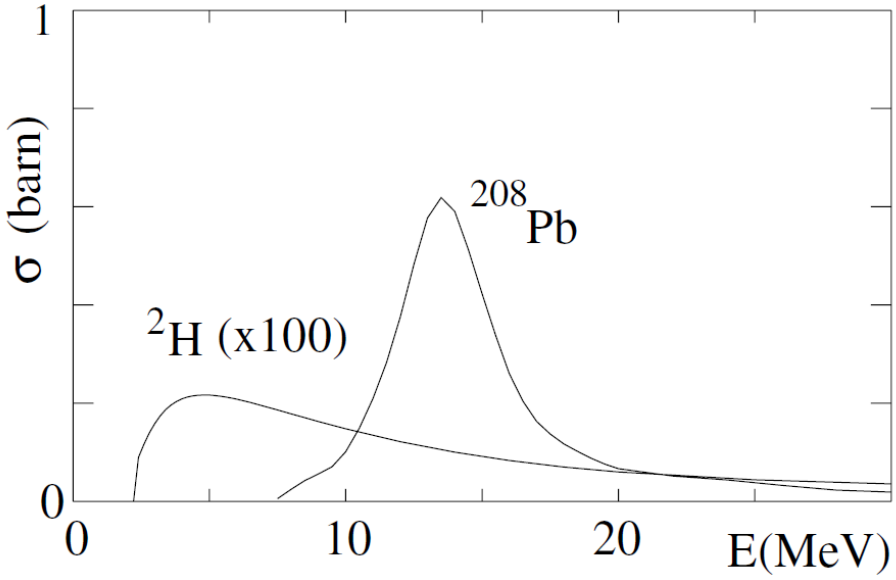

Fig. 3.8. The cross-sections for photo-dissociation of ^{2}H and of ^{208}Pb [30]. The cross-section of Pb exhibits a *giant resonance* typical of heavy nuclei.

Neutrinos Methods for calculating neutrino cross-sections will be presented in Sects. 3.2 and 3.4. Since neutrinos are subject to only weak interactions, their cross sections are considerably smaller than those of other particles. For neutrino energies much less than the masses of the intermediate vector bosons, $m_{\rm W}c^2 = 80.4\,{\rm GeV}$ and $m_{\rm Z}c^2 = 91.2\,{\rm GeV}$ the cross-sections are proportional to the square of the Fermi constant

$$\frac{G_{\rm F}^2}{(\hbar c)^4} \;=\; 5.297\times 10^{-48}\,{\rm m}^2{\rm MeV}^{-2}\;. \tag{3.36}$$

By dimensional analysis, this quantity must be multiplied by the square of an energy to make a cross-section. The cross-sections for several neutrino induced reactions are given in Table 3.1. For nuclear physics, neutrinos of energy $E_\nu \sim 1\,{\rm MeV}$ are typical so, multiplying (3.36) by $1\,{\rm MeV}^2$, gives cross-sections of order $10^{-48}{\rm m}^2$.

Classical scattering on a fixed potential

In this section, we consider the scattering of a particle in a fixed force field described by a potential $V(r)$. This corresponds to situations where the fact that the target particle recoils has little effect on the movement of the beam particle because the kinetic energy of the recoiling target particle can be neglected. For a beam particle of mass $m_{\rm b}$ and momentum $p_{\rm b}$ incident on a target of mass $m_{\rm t}$, it can be shown (Exercise 3.5) that the target recoil has negligible effect if the target rest-energy $m_{\rm t}c^2$ is much greater than the beam energy

$$m_{\rm t}c^2 \;\gg\; E_{\rm b} \;=\; \sqrt{m_{\rm b}^2c^4 + p_{\rm b}^2c^2}\;. \tag{3.37}$$

Table 3.1. The cross-sections for selected neutrino-induced reactions imp for nuclear physics. The energy range where the formulas are valid are given. from G_F^2 given by (3.36), the cross-sections depend on the "weak mixing $\sin^2\theta_w = .2312 \pm 0.0002$, the "Cabibo angle" $\cos\theta_c = 0.975 \pm 0.001$, and the vector coupling" $g_A = 1.267 \pm 0.003$. The meaning of these quantities is dis in Chap. 4.

reaction	cross-section	
$\nu_e\, e^- \rightarrow \nu_e\, e^-$	$\frac{G_F^2 E_{cm}^2}{4\pi(\hbar c)^4}\left[(2\sin^2\theta_w + 1)^2 + \frac{4}{3}\sin^4\theta_w\right]$	$E_{cm} \gg m_e c^2$
$\bar{\nu}_e\, e^- \rightarrow \bar{\nu}_e\, e^-$	$\frac{G_F^2 E_{cm}^2}{4\pi(\hbar c)^4}\left[\frac{1}{3}(2\sin^2\theta_w + 1)^2 + 4\sin^4\theta_w\right]$	$E_{cm} \gg m_e c^2$
$\nu_\mu\, e^- \rightarrow \nu_\mu\, e^-$	$\frac{G_F^2 E_{cm}^2}{4\pi(\hbar c)^4}\left[(2\sin^2\theta_w - 1)^2 + \frac{4}{3}\sin^4\theta_w\right]$	$E_{cm} \gg m_e c^2$
$\bar{\nu}_\mu\, e^- \rightarrow \bar{\nu}_\mu\, e^-$	$\frac{G_F^2 E_{cm}^2}{4\pi(\hbar c)^4}\left[\frac{1}{3}(2\sin^2\theta_w - 1)^2 + 4\sin^4\theta_w\right]$	$E_{cm} \gg m_e c^2$
$\nu_e\, n \rightarrow e^-\, p$	$\frac{G_F^2 E_\nu^2}{\pi(\hbar c)^4}\cos^2\theta_c\left[1 + 3g_A^2\right]$	$m_e c^2 \ll E_\nu \ll m_p c^2$
$\bar{\nu}_e\, p \rightarrow e^+\, n$	$\frac{G_F^2 E_\nu^2}{\pi(\hbar c)^4}\cos^2\theta_c\left[1 + 3g_A^2\right]$	$m_e c^2 \ll E_\nu \ll m_p c^2$

Since nucleons and nuclei are so much heavier than electrons and neutrinos, these conditions will be satisfied in physically interesting situations. This fact, plus the mathematical simplification coming from ignoring target recoil, justifies spending some time on potential scattering. We will therefore first treat the problem classically by following the trajectories of particles through the force field. This will be followed by two quantum-mechanical treatments, the first using perturbation theory and plane waves, and the second using wave packets.

Classical cross-sections

Classically, cross-sections are calculated from the trajectories of particles in force fields. Consider a particle in Fig. 3.9 that passes through a spherically symmetric force field centered on the origin. The particle's original trajectory is parametrized by the "impact parameter" b which would give the particle's distance of closest approach to the force center if there were no scattering.

The scattering angle $\theta(b)$ depends on the impact parameter, as in the figure. The relation $\theta(b)$ or $b(\theta)$ can be calculated by integrating the equations of motion with the initial conditions $p_z = p$, $p_x = p_y = 0$.

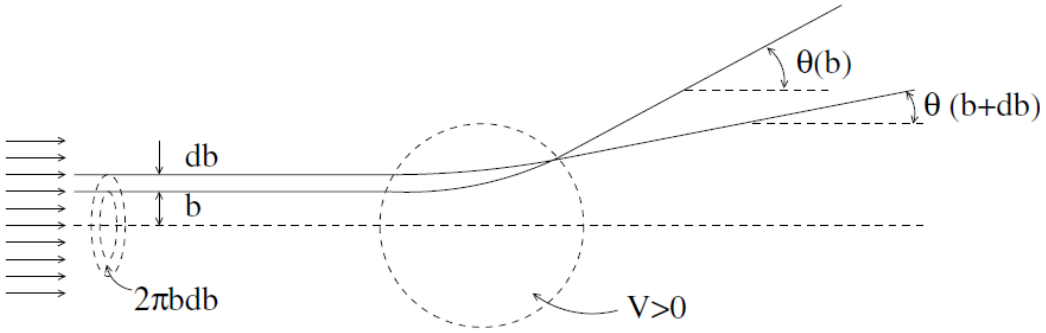

Fig. 3.9. The scattering of a particle of momentum $\boldsymbol{p}$ by a repulsive force. The trajectories for impact parameters b and $b + \mathrm{d}b$ are shown. The probability that a particle is scattered by an angle between $\theta(b)$ and $\theta(b + \mathrm{d}b)$ is proportional to the surface area $2\pi b\mathrm{d}b$.

The probability

that a particle is scattered into an interval $\mathrm{d}\theta$ about θ is proportional to the area of the annular region between $b(\theta)$ and $b(\theta + \mathrm{d}\theta) = b + \mathrm{d}b$, i.e. $\mathrm{d}\sigma = 2\pi b\mathrm{d}b$. The solid angle corresponding to $\mathrm{d}\theta$ is $\mathrm{d}\Omega = 2\pi \sin\theta \mathrm{d}\theta$. The differential elastic scattering cross-section is therefore

$$\frac{\mathrm{d}\sigma}{\mathrm{d}\Omega}(\theta) \;=\; \frac{2\pi b\mathrm{d}b}{2\pi \sin\theta \mathrm{d}\theta} \;=\; \left|\frac{b(\theta)}{\sin\theta} \cdot \frac{db}{d\theta}\right| \quad . \tag{3.38}$$

A measurement of $\mathrm{d}\sigma/\mathrm{d}\Omega$ determines the relation $b(\theta)$ which in turn gives information about the potential V.

Examples

We can apply (3.38) to several simple cases:

- Scattering of a point particle on a hard immovable sphere. The angle-impact parameter relation is

  $$b \;=\; R\cos\theta/2\;, \tag{3.39}$$

  where R is the radius of the sphere. The cross section is then

  $$\frac{\mathrm{d}\sigma}{\mathrm{d}\Omega} = R^2/4 \qquad \Rightarrow \qquad \sigma = \pi R^2 \tag{3.40}$$

  so the total cross-section is just the geometrical cross section of the sphere. In the case of scattering of two spheres of the same radius, the total scattering cross-section is $\sigma = 4\pi R^2$.
- Scattering of a charged particle in a Coulomb potential

  $$V(r) \;=\; \frac{Z_1 Z_2 e^2}{4\pi\epsilon_0 r}\;, \tag{3.41}$$

where Z_1 is the charge of the scattered particle, and Z_2 is the charge of the immobile target particle. This historically important reaction is called "Rutherford scattering" after E. Rutherford who demonstrated the existence of a compact nucleus by studying α-particle scattering on gold nuclei. The unbound orbits in the Coulomb potential are hyperbolas so the scattering angle is well-defined in spite of the infinite range of the force. For an incident kinetic energy $E_k = mv^2/2$, the angle-impact parameter relation is

$$b = \frac{Z_1 Z_2 e^2}{8\pi\epsilon_0 E_k} \cot(\theta/2) \, . \tag{3.42}$$

The cross-section is then

$$\frac{d\sigma}{d\Omega} = \left(\frac{Z_1 Z_2 e^2}{16\pi\epsilon_0 E_k}\right)^2 \frac{1}{\sin^4 \theta/2} \, . \tag{3.43}$$

We note that the total cross-section $\sigma = \int (d\sigma/d\Omega) d\Omega$ diverges because of the large differential cross-section for small-angle scattering:

$$\frac{d\sigma}{d\Omega} \sim \left(\frac{Z_1 Z_2 e^2}{4\pi\epsilon_0 E_k}\right)^2 \frac{1}{\theta^4} \qquad (\theta \ll 1) \, . \tag{3.44}$$

This divergence is due to the fact that incident particles of arbitrarily large impact parameters are deflected. The total elastic cross-section for scattering angles greater than $\theta_{\rm min}$ is (using $\mathrm{d}\Omega \sim 2\pi\theta \mathrm{d}\theta$ for $\theta \ll 1$)

$$\sigma(\theta > \theta_{\rm min}) \sim \left(\frac{Z_1 Z_2 e^2}{4\pi\epsilon_0 E_k}\right)^2 \frac{\pi}{\theta_{\rm min}^2} \qquad (\theta_{\rm min} \ll 1) \, . \tag{3.45}$$

Scattering of particles in a Yukawa potential

$$V(r) = \frac{g\hbar c}{r} \mathrm{e}^{-r/r_0} \, . \tag{3.46}$$

This potential is identical to the Coulomb potential for $r \ll r_0$ but approaches zero much faster for $r > r_0$. Unlike the case of the Coulomb potential, there is no analytical solution for particle trajectories. It is necessary to integrate numerically the equations of motion to find $\theta(b)$ and $\mathrm{d}\sigma/\mathrm{d}\Omega$. The result is shown in Fig. 3.10 for an incident particle of energy $E_k = 10 g\hbar c/r_0$. We see that for $b < r_0$ (corresponding to $\theta > 0.1$) the scattering angle approaches that for the Coulomb potential, as expected since the two potentials have the same form for $r/r_0 \to 0$. For $b > r_0$, the

scattering angle is smaller than the angle for Rutherford scattering since the Yukawa force falls rapidly for $r \gg r_0$. It follows that the differential cross section for small angles is smaller than that for Rutherford scattering, diverging as θ^{-2} rather than as θ^{-4}. The elastic cross section still diverges but only logarithmically, $\sigma(\theta_{\min}) \propto \log(\theta_{\min})$. We see from the figure that

$$\sigma(\theta > 0.01) \;=\; \pi[b(0.01)]^2 \;\sim\; 4\pi r_0^2 \,. \tag{3.47}$$

An angle of 0.01 is already quite small and to get a much higher cross-section one has to go to considerably smaller angles. For the Yukawa potential, πr_0^2 therefore gives the order of magnitude of the cross-section for scattering by measurably large angles. We shall see below that in the quantum-mechanical calculation, the cross-section is finite.

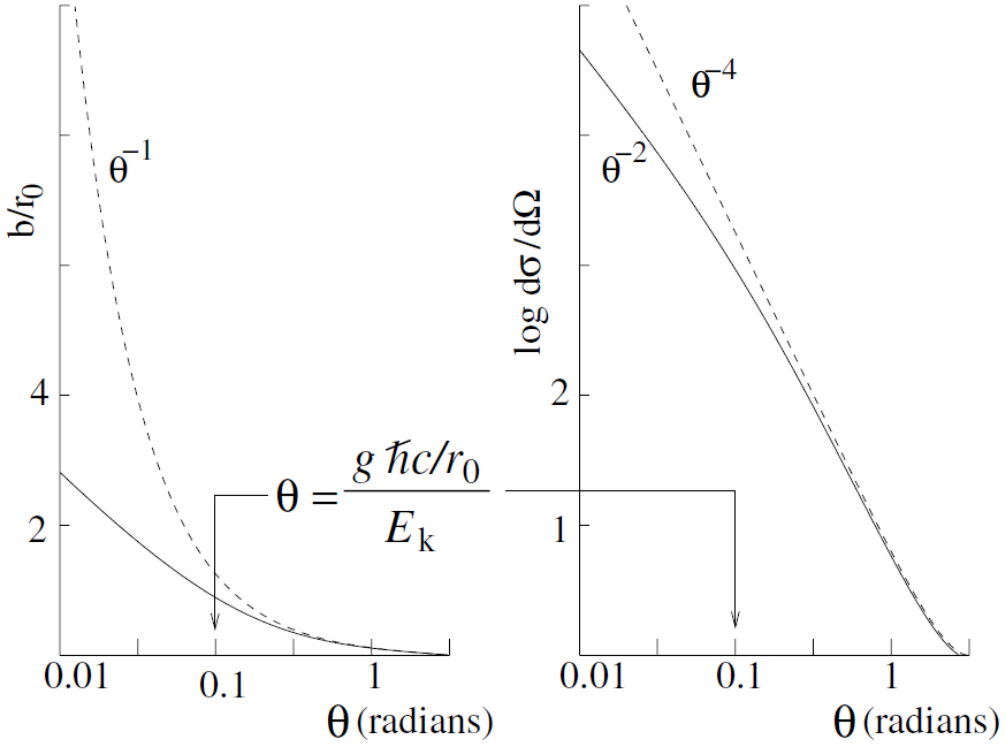

Fig. 3.10. The scattering of a non-relativistic particle in a Yukawa potential $V(r) = g\hbar c\, e^{-r/r_0}/r$. The initial kinetic energy of the particle is taken to be $10g\hbar c/r_0$ so that it can penetrate to about $r = r_0/10$. The left solid curve shows the numerically calculated impact parameter $b(\theta)$ in units of r_0. The right solid curve shows the logarithm of the differential scattering normalized to the backward scattering cross-section ($\theta = \pi$). For comparison, the dashed lines show the same functions for the Coulomb potential $V(r) = g\hbar c/r$. For $\theta > 0.1$, we have $b < r_0$ and the two potentials give nearly the same results. This is to be expected since the two potentials are nearly equal for $r \ll r_0$. For $b \gg r_0$, the Yukawa scattering angle is much less than the Coulomb scattering angle because the force drops of much faster with distance. As a consequence, the cross section is smaller.

Much of our knowledge of nuclear structure comes from the scattering of charged particles (generally electrons) on nuclei. This is because high-energy charged particles penetrate inside the nucleus and their scattering-angle distribution therefore gives information on the distribution of charge in the nucleus. We will see that the correct interpretation of these experiments requires quantum-mechanical calculation of the cross-sections. However, it turns out that the quantum-mechanical calculation of scattering in a $1/r$ potential gives the same result as the classical Rutherford cross-section found above. This means that the Rutherford cross-section can be used to interpret experiments using positively charged particles whose energy is sufficiently low that they cannot penetrate inside the nucleus.

This is how, in 1908, Rutherford discovered that the positive charge inside atoms is contained in a small "nucleus." Rutherford reached this conclusion after hearing of the results of experiments by Geiger and Marsden studying the scattering of α-particles on gold foils. While most α's scattered into the forward direction, they occasionally scatter backward. This was impossible to explain with the then popular "plum pudding" model advocated by J.J. Thomson where the atom consisted of electrons held within a positively charged uniform material. A heavy α-particle cannot be deflected through a significant angle by the much lighter electron. On the other hand, scattering at large angle would be possible in rare nearly head-on collisions with a massive, and therefore immobile, gold nucleus.

After this brilliant insight, Rutherford spent some time (2 weeks [5]) calculating the expected angular distribution which turned out to agree nicely with the observed distribution. Rutherford's model naturally placed the light electrons in orbits around the heavy nucleus.

Another 17 years were necessary to develop the quantum mechanics that explains atomic structure and dynamics.

We expect the Rutherford cross-section calculation to fail if the electron can penetrate inside the nucleus. Classically, this will happen for head-on collisions if the initial kinetic energy of the α particle is greater than the electrostatic potential at the nuclear surface:

$$E_k = \frac{2Ze^2}{4\pi\epsilon_0 R} = \frac{2Z\alpha\hbar c}{R} \sim 1.2\, A^{2/3}\,\mathrm{MeV}\,, \tag{3.48}$$

where $2Z$ is the product of the α-particle and nuclear charges, α is the fine structure constant, and we have used $R \sim 1.2A^{1/3}\,\mathrm{fm}$ and $Z \sim A/2$. We expect the backward scattering to be suppressed for energies greater than this value. The naturally occurring α-particles used by Rutherford have energies of order 6 MeV so the effect can only be seen for $Z/A^{1/3} < 3$ corresponding to $A < 11$. Rutherford and collaborators used this effect to perform the first measurement of nuclear radii.

Quantum mechanical scattering on a fixed potential

In this section, we consider two simple approximate methods applicable to scattering due to weak and electromagnetic interactions. The first uses standard time-dependent perturbation theory applied to momentum eigenstates and the second uses wave packets. The first is an essential part of this chapter because it can be easily generalized to inelastic scattering. The second is mostly a parenthetical section intended to improve our understanding of the physics.

To prepare the ground for the perturbation calculation, we first briefly discuss the concept of *asymptotic states* and their normalization. Other technical ingredients, the limiting forms of the Dirac δ function, and basics results of time-dependent perturbation theory in quantum mechanics are reviewed in Appendix C.

Asymptotic states and their normalization

In studying nuclear, or elementary interactions, we are most of the time not interested in a space-time description of phenomena.[2] Instead, we study processes in which we prepare initial particles with definite momenta and far away from one another so that they are out of reach of their interactions at an initial time t_0 in the "distant past" $t_0 \sim -\infty$. We then study the nature and the momentum distributions of final particles when these are also out of range of the interactions at some later time t in the "distant future" $t \to +\infty$. (The size of the interaction region is of the order of 1 fm, the measuring devices have sizes of the order of a few meters.)

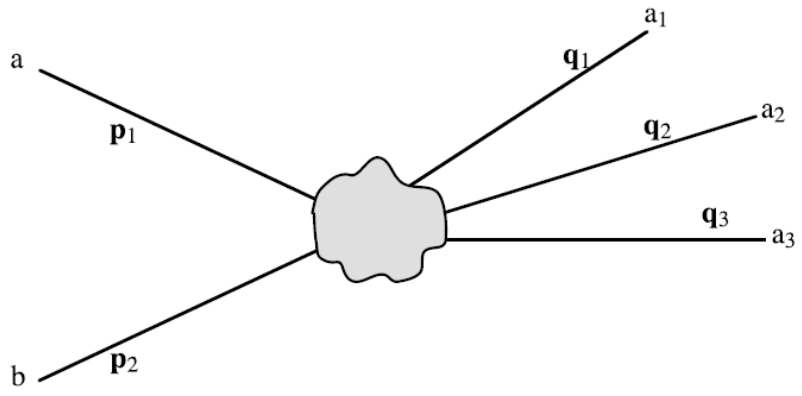

Fig. 3.11. Asymptotic states in a collision

Under these assumptions, the initial and final states of the particles under consideration are *free* particle states. These states are called *asymptotic states*. The decay of an unstable particle is a particular case. We measure the energy and momenta of final particles in asymptotic states.

By definition, the asymptotic states of particles have definite momenta. Therefore, strictly speaking, they are not physical states, and their wave functions $e^{ipx/\hbar}$ are not square integrable. Physically, this means that we are actually interested in wave packets who have a non vanishing but very small extension Δp in momentum, i.e. $\Delta p/|p| \ll 1$.

It is possible to work with plane waves, provided one introduces a proper normalization. A limiting procedure, after all calculations are done, allows to get rid of the intermediate regularizing parameters. This is particularly simple in first order Born approximation, which we will present first. The complete manipulation of wave packets is possible but somewhat complicated. However, it gives interesting physical explanations for various specific problems, and we shall discuss it in Sect. 3.3.5.

We will consider that the particles are confined in a (very large but finite) box of volume L^3. We will let L tend to infinity at the end of the calculation. Besides its simplicity, this procedure allows to incorporate relativistic kinematics of ingoing and outgoing particles in a simple manner.

In such a box of size L, the normalized momentum eigenstates are

$$|\boldsymbol{p}\rangle \to \psi_{\boldsymbol{p}}(\boldsymbol{r}) = L^{-3/2} e^{i\boldsymbol{p}\cdot\boldsymbol{r}/\hbar} \quad \text{inside the box} \quad , \tag{3.49}$$

$$\psi_{\boldsymbol{p}}(\boldsymbol{r}) = 0 \quad \text{outside the box} \quad .$$

These wave functions are normalized in the sense that

$$\int |\psi_{\boldsymbol{p}}(\boldsymbol{r})|^2 \, d^3\boldsymbol{r} \; = \; 1 \; . \tag{3.50}$$

For convenience, we will define here the Hilbert space with *periodic* boundary conditions : in one dimension $\psi(L/2) = \psi(-L/2)$ and $\psi'(L/2) = \psi'(-L/2)$ (this amounts to quantizing the motion of particles on a large circle of radius $R = L/2\pi$). In such conditions, the operators $\hat{p} = (\hbar/i)\partial/\partial x$ and $\hat{p}^2$ have a discrete spectrum $p_n = 2\pi n\hbar/L$. In three dimensions the quantization of momentum is $\boldsymbol{p} = (2\pi\hbar/L)(n_1, n_2, n_3)$, where the n_i are arbitrary integers.

The advantage of using periodic boundary conditions is that the states (3.49) are normalized eigenstates of *both* the energy and the momentum, as we wish. This is not the case in the usual treatment of a "particle in a box" where one requires that the wave function vanish at the edge of the box. The energy eigenfunctions in this case are

$$\psi_E(\boldsymbol{r}) \; = \; L^{-3/2} \sin n_x \pi x/L \; \sin n_y \pi y/L \; \sin n_z \pi z/L \tag{3.51}$$

where n_x, n_y, n_z are positive integers and $E = \pi^2\hbar^2(n_x^2 + n_y^2 + n_z^2)/2mL^2$. In this case the energy eigenfunctions are not eigenstates of momentum. However, both boundary conditions give the same density of states so we need not worry about which regularization procedure is used.

The orthogonality relation between momentum eigenstates

$$\langle \boldsymbol{p}|\boldsymbol{p}'\rangle = \delta_{n_1 n_1'}\delta_{n_2 n_2'}\delta_{n_3 n_3'}$$

can also be written in the following manner, useful to take limits,

$$\langle \boldsymbol{p}|\boldsymbol{p}'\rangle = (2\pi\hbar/L)^3 \Delta_L^3(\boldsymbol{p}-\boldsymbol{p}') \quad , \tag{3.52}$$

where $\Delta_L^3(\boldsymbol{p}-\boldsymbol{p}')$ is a limiting form of the delta function discussed in Appendix (C.0.2).

Since each component of momentum is quantized in steps of $2\pi\hbar/L$, the number of states in a momentum volume $\mathrm{d}^3\boldsymbol{p}$ is

$$\mathrm{d}N(\boldsymbol{p}) \;=\; (2s+1)(\frac{L}{2\pi\hbar})^3 \mathrm{d}^3\boldsymbol{p} \;\equiv\; \rho(\boldsymbol{p})\mathrm{d}^3\boldsymbol{p} \tag{3.53}$$

where $2s+1$ is the number of spin-states for a particle of spin s. This defines the *density of states* (in momentum space): $\rho(\boldsymbol{p}) = (2s+1)(L/2\pi\hbar)^3$. This corresponds to a density in *phase space* (momentum×real space) of $(2s+1)$ states per elementary volume $(2\pi\hbar)^3$.

In what follows, we will be interested in the number of states in an interval $\mathrm{d}E$. To obtain this, we note that the number of states within a momentum volume $\mathrm{d}^3\boldsymbol{p}$ can be written as

$$\mathrm{d}N(\boldsymbol{p}) \;=\; \rho(\boldsymbol{p})\mathrm{d}^3\boldsymbol{p} \;=\; (2s+1)(\frac{L}{2\pi\hbar})^3\, p^2\mathrm{d}p\mathrm{d}\Omega \;, \tag{3.54}$$

where $\mathrm{d}\Omega$ is the solid angle covered by $\mathrm{d}^3\boldsymbol{p}$. Taking $E\mathrm{d}E = c^2\, p\mathrm{d}p$ (which holds both in the relativistic and non-relativistic regimes), we find the number of states in the interval $\mathrm{d}E$ and in the solid angle $\mathrm{d}\Omega$ is

$$\mathrm{d}N(E,\mathrm{d}\Omega) \;=\; (2s+1)(\frac{L}{2\pi\hbar})^3\, \frac{pE}{c^2}\mathrm{d}E\mathrm{d}\Omega \;. \tag{3.55}$$

Cross-sections in quantum perturbation theory

The simplest way to calculate cross-sections in quantum mechanics is to use standard time-dependent perturbation theory (Appendix C). The idea is to describe the system by a Hamiltonian that is the sum of an "unperturbed" H_0 and a perturbation H_1. In the present context, H_0 will represent the kinetic energy of the incoming and outgoing beam particles and the perturbation H_1 will be the interaction potential (which acts for a very short time).

Perturbation theory gives the transition rates between energy eigenstates of the unperturbed Hamiltonian, i.e. between the initial state $|i\rangle$ of energy E_i and one of the possible final states $|f\rangle$ of energy E_f. The first order result

is

$$\lambda_{i\to f} \;=\; \frac{2\pi}{\hbar}\,|\langle f|H_1|i\rangle|^2\,\delta(E_f - E_i)\;, \tag{3.56}$$

where $\delta(E)$ satisfies

$$\int_{-\infty}^{\infty}\delta(E)\mathrm{d}E \;=\; 1\;, \tag{3.57}$$

and is a limiting form of the delta function discussed in (C.0.2). The dimension of $\delta(E)$ is 1/energy so the transition rate λ has dimension of 1/time as expected.

If higher-order perturbation theory is necessary, energy will still be conserved in the transition rate since energy conservation is an exact result due to the time-translation invariance of the Hamiltonian. The more general transition rate including higher-order effects is then written as

$$\lambda_{i\to f} \;=\; \frac{2\pi}{\hbar}\,|\langle f|T|i\rangle|^2\,\delta(E_f - E_i)\;, \tag{3.58}$$

where T is the "transition matrix element." In the context of scattering theory, the first order result, $T = H_1$, is called the "Born approximation."

For the initial and final states, we choose plane waves of momentum $\boldsymbol{p}$ and $\boldsymbol{p}'$ as defined above

$$\psi_i(\boldsymbol{r}) \;=\; \frac{\mathrm{e}^{\mathrm{i}\boldsymbol{p}\cdot\boldsymbol{r}/\hbar}}{L^{3/2}} \qquad \psi_f(\boldsymbol{r}) \;=\; \frac{\mathrm{e}^{\mathrm{i}\boldsymbol{p}'\cdot\boldsymbol{r}/\hbar}}{L^{3/2}}\;, \tag{3.59}$$

where L^3 is the normalization volume. The classical scattering angle is defined by

$$\cos\theta \;=\; \frac{\boldsymbol{p}\cdot\boldsymbol{p}'}{|\boldsymbol{p}||\boldsymbol{p}'|}\;. \tag{3.60}$$

Of more importance for quantum calculations is the momentum transfer

$$\boldsymbol{q} \;=\; \boldsymbol{p}' - \boldsymbol{p}\;, \tag{3.61}$$

and its square

$$\boldsymbol{q}^2 \;=\; \boldsymbol{q}\cdot\boldsymbol{q} \;=\; |\boldsymbol{p}|^2 \,+\, |\boldsymbol{p}'|^2 \,-\, 2\boldsymbol{p}\cdot\boldsymbol{p}'\;. \tag{3.62}$$

For elastic scattering we have $|\boldsymbol{p}| = |\boldsymbol{p}'| = p$ so

$$\boldsymbol{q}^2 \;=\; 2p^2(1-\cos\theta) \;=\; 4p^2\sin^2\theta/2 \quad \text{(elastic scattering)}\;. \tag{3.63}$$

The small angle limit is often useful:

$$\boldsymbol{q}^2 \sim p^2\theta^2 \quad \theta \ll 1\,, \quad \text{(elastic scattering)}\,. \tag{3.64}$$

The matrix element between initial and final states is then

$$\langle \boldsymbol{p}'|V|\boldsymbol{p}\rangle = \frac{1}{L^3}\int \mathrm{e}^{\mathrm{i}(\boldsymbol{p}-\boldsymbol{p}')\cdot\boldsymbol{r}/\hbar}V(\boldsymbol{r})\mathrm{d}^3\boldsymbol{r} = \frac{\tilde{V}(\boldsymbol{p}-\boldsymbol{p}')}{L^3}\,. \tag{3.65}$$

It is proportional to the Fourier transform of the potential

$$\tilde{V}(\boldsymbol{q}) \;=\; \int \mathrm{e}^{\mathrm{i}\boldsymbol{q}\cdot\boldsymbol{r}/\hbar}\,V(\boldsymbol{r})\mathrm{d}^3\boldsymbol{r}\,. \tag{3.66}$$

Note that the dimensions of $\tilde{V}$ defined here are energy×volume.

The transition rate to the final state is

$$\lambda_{i\to f} \;=\; \frac{2\pi}{\hbar}\frac{|\tilde{V}(\boldsymbol{p}-\boldsymbol{p}')|^2}{L^6}\delta(E'-E)\,. \tag{3.67}$$

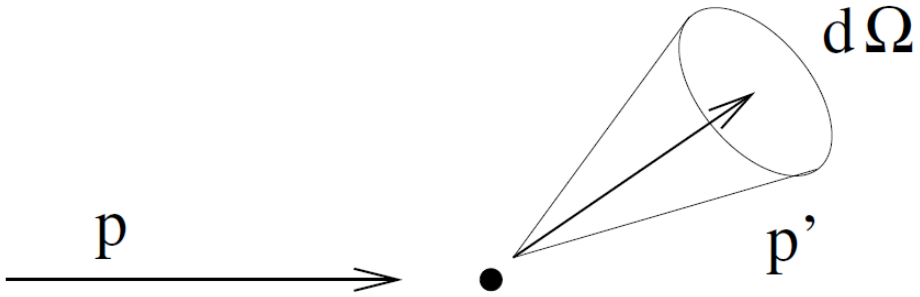

Fig. 3.12. Scattering of a single particle by a fixed potential.

We cannot measure the transition rate to a *single* momentum state so we must sum the transition rate over a group of interesting final states. Within a volume L^3, the number of momentum states in the momentum range $\mathrm{d}^3\boldsymbol{p}'$ is given by (3.53). Multiplying (3.67) by this number of states we get the total transition rate into the momentum volume $\mathrm{d}^3\boldsymbol{p}$

$$\lambda(\mathrm{d}^3\boldsymbol{p}') \;=\; \left(\frac{L}{2\pi\hbar}\right)^3 \mathrm{d}^3\boldsymbol{p}'\,\frac{2\pi}{\hbar}\frac{|\tilde{V}(\boldsymbol{q})|^2}{L^6}\delta(E'-E)\,. \tag{3.68}$$

We carefully drop the factor $(2s+1)$ in the number of states. We do this because it is often the case that only one spin state is produced with high probability in a reaction. When this is not the case, it is then necessary to sum over all possible final spin states.

The number of states in the momentum range $\mathrm{d}E'$ and momentum oriented into the solid angle $\mathrm{d}\Omega$ at angles (θ, ϕ) with respect to a given direction is given by (3.55) so the total transition rate into these states is then

$$\lambda(\mathrm{d}E', \mathrm{d}\Omega) \;=\; \left(\frac{L}{2\pi\hbar}\right)^3 \frac{p'E'}{c^2}\mathrm{d}E'\mathrm{d}\Omega \frac{2\pi}{\hbar}\frac{|\tilde{V}(\boldsymbol{q})|^2}{L^6}\delta(E'-E)\;. \tag{3.69}$$

We use the delta function to integrate over energy in order to find the transition rate into (energy-conserving) states within the solid angle $\mathrm{d}\Omega$

$$\lambda(\mathrm{d}\Omega) \;=\; \frac{v'}{L^3}\frac{(E')^2}{4\pi^2\hbar^4c^4}\,|\tilde{V}(\boldsymbol{q})|^2\,\mathrm{d}\Omega\;, \tag{3.70}$$

where $v' = p'c^2/E'$ is the velocity of the final state particle.

We remark, as mentioned above, that the crucial factor in (3.70) is the presence of the modulus squared of the Fourier transform of the potential $|\tilde{V}(\boldsymbol{q})|^2$. This is the main result of this calculation. Information on the differential cross-section gives us direct access to the potential through its Fourier transform. This result is very concise and elegant. It is basically the same effect that one encounters in diffraction phenomena. If one neglects multiple scattering, the amplitude of the diffraction pattern is the Fourier transform of the diffracting system (crystal, macro-molecule, etc.).

Elastic scattering

For elastic scattering, $E' = E$, so the transition rate is

$$\lambda(\mathrm{d}\Omega) \;=\; \frac{v}{L^3}\frac{E^2}{4\pi^2\hbar^4c^4}\,|\tilde{V}(\boldsymbol{q})|^2\,\mathrm{d}\Omega\;, \tag{3.71}$$

where v is the velocity of the initial state particle. The transition rate is proportional to the density of scattering centers ($n = 1/L^3$) and to the velocity of the projectile. Using (3.30), we divide by these two factors to get the differential cross-section

$$\frac{d\sigma}{d\Omega} \;=\; \frac{E^2}{4\pi^2(\hbar c)^4}|\tilde{V}(\boldsymbol{q})|^2\;, \tag{3.72}$$

where $E = \sqrt{p^2c^2 + m^2c^4}$ is the energy of the incident particle and $\tilde{V}$ is given by (3.66).

We remark that in the above expression the normalization parameter L cancels off identically. Therefore, we can readily take the limit $L \to \infty$.

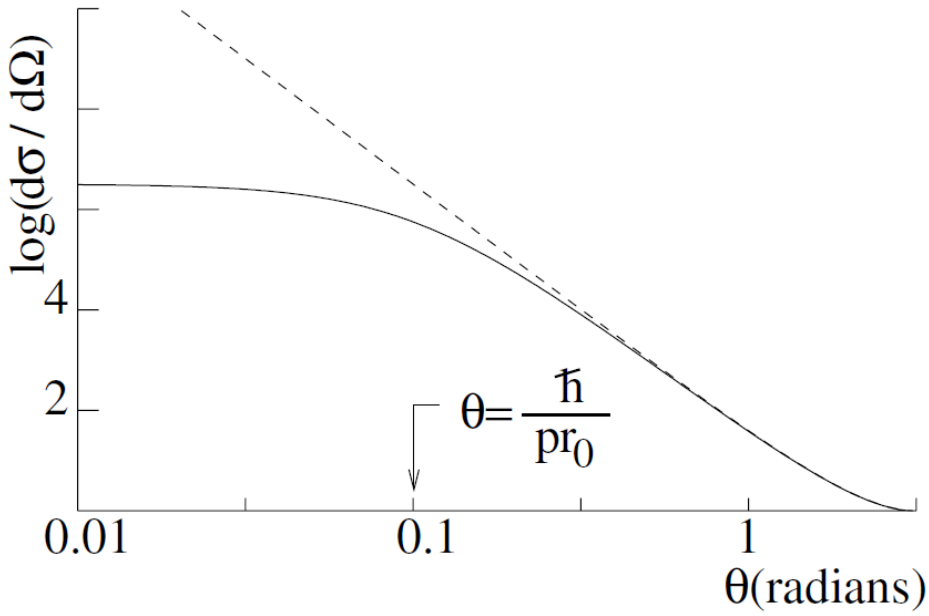

Fig. 3.13. The scattering of a non-relativistic particle in a Yukawa potential $V(r) = g\hbar c\mathrm{e}^{-r/r_0}/r$. The momentum of the particle is $p = 10\hbar/r_0$. The solid line shows the quantum mechanical differential cross-section (3.75). For small angles $\theta < \hbar/(pr_0)$ the cross section is flat, avoiding the divergence present in the classical calculation (Fig. 3.10). At large angles $\theta > \hbar/(pr_0)$ the scattering follows the Coulomb cross-section shown by the dashed line.

As an example of potential scattering, we can take the Yukawa potential

$$V(r) = \frac{g\hbar c}{r}\,\mathrm{e}^{-r/r_0}\ , \tag{3.73}$$

where the range of the interaction is the Compton wavelength $r_0 = \hbar/Mc$ of the exchanged particle of mass M. The Coulomb potential between particles of charge Z_1 and Z_2 corresponds to $g = Z_1 Z_2 \alpha$ and $r_0 \to \infty$. The Fourier transform $\tilde{V}(\boldsymbol{q})$ for the Yukawa potential is

$$\tilde{V}(\boldsymbol{q}) = \frac{4\pi\, g\hbar c\,\hbar^2}{\boldsymbol{q}^2 + (\hbar/r_0)^2} = \frac{4\pi g(\hbar c)^3}{\boldsymbol{q}^2c^2 \,+\, M^2c^4}\quad , \tag{3.74}$$

which gives a differential cross-section

$$\frac{\mathrm{d}\sigma}{\mathrm{d}\Omega} \;=\; 4g^2(\hbar c)^2\left(\frac{E}{4p^2c^2\sin^2\theta/2 \,+\, M^2c^4}\right)^2\ , \tag{3.75}$$

where we have used (3.63). The cross section, shown in Fig. 3.13, does not diverge at small angles like the classical cross-section. The total elastic cross-section is therefore finite:

$$\sigma_{\mathrm{el}} \;=\; 8\pi g^2\,(\hbar c)^2\left(\frac{E}{M^2c^4}\right)^2\frac{1}{1+2p^2/M^2c^2}\ . \tag{3.76}$$

We remark that in many strong interaction calculations, the Born approximation is not valid. Indeed the dimensionless parameter g is larger than one and perturbation theory does not apply. Nevertheless, the above result bears many qualitatively useful features.

In what follows, we consider cases where the Born approximation is valid. There are two simple limits corresponding to the mass of the exchanged particle Mc^2 being much greater than or much less than pc.

- $Mc^2 \ll pc$, i.e. $r_0 \gg \hbar/p$. As illustrated in Fig. 3.13, the differential cross section is angle-independent for $\theta < \hbar/(pr_0)$ and Rutherford-like for $\theta > \hbar/(pr_0)$. We can then find the cross-section for the Coulomb potential by taking the limit $r_0 \to \infty$ and setting $g = Z_1 Z_2 \alpha$:

$$\frac{d\sigma}{d\Omega} = \left(\frac{Z_1 Z_2 e^2}{4\pi\epsilon_0}\right)^2 \left(\frac{E}{2p^2c^2}\right)^2 \frac{1}{\sin^4\theta/2} \quad . \tag{3.77}$$

  In the non-relativistic limit, $E = mc^2$, $E_\mathrm{k} = p^2/2m$, and the formula reduces to the classical Rutherford cross-section (3.43).

$$\frac{d\sigma}{d\Omega} = \left(\frac{Z_1 Z_2 e^2}{16\pi\epsilon_0}\right)^2 \left(\frac{1}{p^2/2m}\right)^2 \frac{1}{\sin^4\theta/2} \quad . \tag{3.78}$$

  This coincidence of the classical and the quantum theory seems, at first, amazing. It is actually quite simple to understand by dimensional analysis. The non-relativistic cross-section (3.78) calculated quantum mechanically turns out to be independent of $\hbar$. It is proportional to the square of the *only* length, $a = e^2/4\pi\epsilon_0(p^2/2m)$, that is linear in $e^2/4\pi\epsilon_0$ and a combination of powers of p, m and $\hbar$. Since this is the only length available, the

quantum cross-section must be $\hbar$-independent and can therefore agree with a classical cross-section, also $\hbar$-independent.[3] The same is not true for the Yukawa potential where the differential cross-section derived from (3.74) depends on $\hbar$ and consequently *cannot* agree with the classical calculation, as seen by comparing Figs. (3.10) and (3.13). It is the existence of another length scale, r_0, that allows one to form a cross-section that depends on $\hbar$.

In the case where the incident particle is ultra-relativistic, $E \sim pc$, we have

$$\frac{d\sigma}{d\Omega} = \left(\frac{Z_1 Z_2 \alpha}{2}\right)^2 \left(\frac{\hbar c}{E}\right)^2 \frac{1}{\sin^4\theta/2} \quad . \tag{3.79}$$

The cross-section is proportional to α^2 and to the square of the only length, $\hbar c/E$, that can be formed from $\hbar$, c, and E. (In the relativistic limit, the cross-section no longer depends on m.)

- $Mc^2 \gg pc$, i.e. $r_0 \ll \hbar/p$. In this case, the differential cross-section is angle-independent for all θ

$$\frac{\mathrm{d}\sigma}{\mathrm{d}\Omega} = \frac{G^2E^2}{4\pi^2(\hbar c)^4} \quad \text{i.e.} \quad \sigma = \frac{G^2E^2}{\pi(\hbar c)^4} \quad , \tag{3.80}$$

where

$$G \;=\; 4\pi\,\frac{g(\hbar c)^3}{(Mc^2)^2}\;. \tag{3.81}$$

Not surprisingly, this cross-section results also from the delta potential, i.e. a contact interaction.

$$V(r) \;=\; G\delta^3(\boldsymbol{r}) \qquad \Rightarrow \tilde{V}(\boldsymbol{q}) \;=\; G\;. \tag{3.82}$$

This potential is a good approximation for neutrino interactions like

$$\nu_e e^- \;\rightarrow\; \nu_e e^-\;. \tag{3.83}$$

From Table 3.1, we see that in this case $G \propto G_F$ where G_F is the Fermi constant.

---

[3] Another puzzle lies in the fact that (3.77), which obtained in perturbation theory, actually coincides with the exact non-relativistic result, which can be calculated analytically with the Schödinger equation (see for instance A. Messiah, *Quantum Mechanics* vol. 1, chap. XI-7). This "miraculous" coincidence comes from the fact that since Coulomb forces are long range forces, one is not allowed, in principle, to make use of plane waves as asymptotic states. One should rather use Coulomb wavefunctions, defined in Messiah, as asymptotic states. The miracle is that the sum of the correct perturbation series gives exactly the simple plane-wave formula. This is again related to the fact that $\hbar$ is absent in the classical result.

Quasi-elastic scattering

Potential scattering most naturally applies to elastic scattering because of the classical limit of a light particle moving through the force field of a fixed heavy particle. However, in the quantum treatment, we saw that the potential simply serves to calculate a matrix element between initial and final states. It is not surprising therefore that the same formalism applies to "quasi-elastic" scattering where the light particle changes its nature (i.e. its mass) when it interacts with a fixed particle. Obvious candidates are the weak interactions of leptons scattering on nucleons, e.g.

$$\bar{\nu}_e\, p \;\leftrightarrow\; e^+\, n\;. \tag{3.84}$$

We note that the reaction going to the right is endothermic and the reaction going to the left is exothermic. Since these two reactions are due to the exchange of W bosons, we can use a delta-potential of the form (3.82) and rely on the fundamental theory of weak interactions (Table 3.1) to provide us with the effective G for each reaction.

The rate calculation proceeds as in the elastic case up to (3.70) at which point we have to take into account the fact the the initial and final state momenta are not equal. Since we will want to factor out the initial state velocity, we write the rate as

$$\lambda(\mathrm{d}\Omega) \;=\; \frac{v}{L^3}\frac{v'}{v}\frac{(E')^2}{4\pi^2\hbar^4c^4}\,|\tilde{V}(\boldsymbol{q})|^2\,\mathrm{d}\Omega\;, \tag{3.85}$$

corresponding to a cross-section

$$\frac{\mathrm{d}\sigma}{\mathrm{d}\Omega} \;=\; \frac{v'}{v}\frac{(E')^2}{4\pi^2\hbar^4c^4}\,|\tilde{V}(\boldsymbol{q})|^2\;. \tag{3.86}$$

For the delta-potential, the angular distribution is isotropic and the cross-section is

$$\sigma \;=\; \frac{v'}{v}\frac{(E')^2}{\pi\hbar^4c^4}\,G^2\;. \tag{3.87}$$

At sufficiently high energy, the initial and final state velocities approach c so the factor v'/v is of no importance. At low energy, this factor generates a very different behavior for the two reactions.

The endothermic reaction $\bar{\nu}_\mathrm{e}\mathrm{p} \to \mathrm{e}^+\mathrm{n}$ has a threshold neutrino energy of $E_\mathrm{th} = (m_\mathrm{n} + m_\mathrm{e} - m_\mathrm{p})c^2 = 1.8\,\mathrm{MeV}$. Near threshold, the final state positron has an energy $E' \sim m_\mathrm{e}c^2$ and a velocity $v' \sim \sqrt{2(E_\nu - E_\mathrm{th})/m_\mathrm{e}}$. The initial velocity for the nearly massless neutrino is $v \sim c$ so the cross-section is

$$\sigma \;=\; \left(\frac{2(E_\nu - E_\mathrm{th})}{m_\mathrm{e}c^2}\right)^{1/2}\frac{(m_\mathrm{e}c^2)^2}{\pi\hbar^4c^4}\,G^2 \qquad E_\nu > E_\mathrm{th}\;. \tag{3.88}$$

The situation for the exothermic reaction $\mathrm{e}^+\mathrm{n} \to \bar{\nu}_\mathrm{e}\mathrm{p}$ is quite different. As the velocity v of the positron approaches zero, the energy E' of the final state neutrino approaches $(m_\mathrm{n} + m_\mathrm{e} - m_\mathrm{p})c^2 = 1.8\,\mathrm{MeV}$ so the cross-section approaches

$$\sigma \;=\; \frac{c}{v}\frac{(m_\mathrm{n} + m_\mathrm{e} - m_\mathrm{p})^2c^4}{\pi\hbar^4c^4}\,G^2\;. \tag{3.89}$$

The cross-section is proportional to the inverse of the velocity, as anticipated in Sect. 3.1.5. The reaction rate, proportional to the product of the velocity and the cross-section is therefore velocity independent.

Scattering of quantum wave packets

The calculations of the last section were very efficient in yielding reaction rates and cross-sections in cases where perturbation theory applies. However, they are not able to elicit various physical properties of interest. In this section, we will provide a more physical description using wave packets, which we shall use later on.

In quantum mechanics, particles are represented by wavefunctions, $\psi(\boldsymbol{r})$ giving the probability $|\psi(\boldsymbol{r})|^2 \mathrm{d}^3 r$ to find the particle in a volume $\mathrm{d}^3 r$ near $\boldsymbol{r}$. If the particle interacts only via a potential $V(r)$, the wavefunction satisfies the Schrödinger equation

$$\mathrm{i}\hbar \frac{\partial \psi}{\partial t} = \frac{-\hbar^2}{2m} \nabla^2 \psi + V(r)\psi \, . \tag{3.90}$$

As illustrated in Fig. 3.14, a scattering experiment on a single target particle with a short range potential corresponds to the situation where $V(r) \sim 0$ except in a small region $r < R$ near the target particle. Initially, the wavefunction is a broad wave packet, ψ_{in}, that propagates freely in the z direction far from the target. The transverse width of the wave packet is taken to be much greater than R so that the entire potential is "sampled" by the wavefunction. When the wave packet reaches the target ($t = 0$), the interaction with the potential generates a scattered wave packet ψ_{sc} which now accompanies the transmitted wave packet.

The essential result of the calculation that follows is that the scattered wave is found by summing spherical waves emanating from each point in the region where $V \neq 0$. This is illustrated in Fig. 3.15. It will turn out that the scattered wave from each point is proportional to the product of the potential and the incident wave at that point. This is physically reasonable since the scattered wave must vanish when either the potential or the incident wave vanishes. When one integrates the waves over the region of non-vanishing potential, the result (3.113) that the scattered wave is proportional to the Fourier transform of the potential will emerge in a natural way. Physically, this comes about since, as illustrated in Fig. 3.15, the waves add coherently in the forward direction but with increasingly random phases away from the forward direction. This leads to a decreasing cross-section with increasing angle. Mathematically, this is just what the Fourier transform does since it is maximized at $\boldsymbol{q} = 0$ ($\theta = 0$).

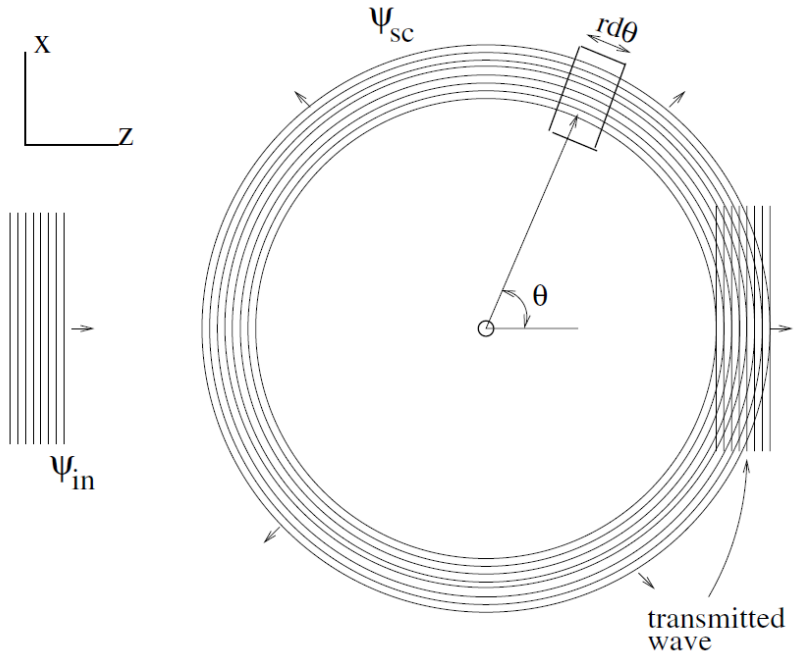

Fig. 3.14. A wave packet that impinges upon a region with $V(r) \neq 0$ will interact in a way that will produce a scattered wave packet and a transmitted wave packet. The probability to find the particle in the box in the scattered wave is proportional to the differential scattering cross-section, $\mathrm{d}\sigma/\mathrm{d}\Omega$.

We now start the wave packet calculation of the differential cross-section. This cross-section is related to the rate of particles counted by a detector placed at an angle θ with respect to the beam shown in Fig. 3.14. The rate is given by

$$\frac{\mathrm{d}N_{\mathrm{det}}}{\mathrm{d}t} = N_{\mathrm{T}}\, F\, \frac{\mathrm{d}\sigma}{\mathrm{d}\Omega}\mathrm{d}\Omega\,, \tag{3.91}$$

where N_{T} is the number of target particles and F is the incident particle flux. We average the flux over some arbitrary time T much greater than the time of passage of the wave packet. The mean incident flux is given by the probability to find the incident particle near the z-axis:

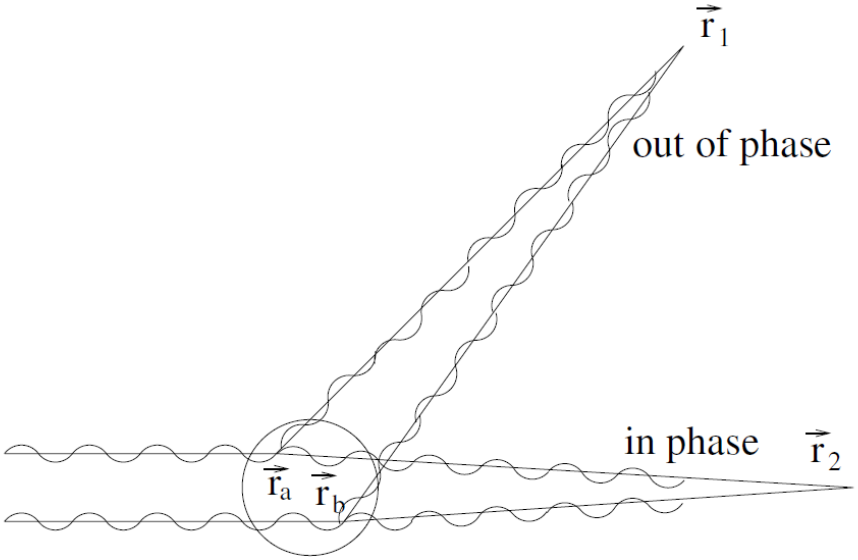

Fig 3.15

Fig. 3.15. In the Born approximation, the scattered wave at any point far from the region of $V \neq 0$ is the sum of spherical waves emitted at each point $\boldsymbol{r}'$ in the scattering region. The figure shows who such waves, one emitted at $\boldsymbol{r}_a$ and one at $\boldsymbol{r}_b$. The phase of the scattered wave at the point $\boldsymbol{r}$ is $k(z' + |\boldsymbol{r} - \boldsymbol{r}'|)$. Only in the forward direction is this phase independent of $\boldsymbol{r}'$. In other directions, the phase depends on $\boldsymbol{r}'$ so the spherical waves do not sum coherently. This results in a diminishing of the cross-section for angles satisfying $|\boldsymbol{p}' - \boldsymbol{p}|R > \hbar$.

$$F(x = y = 0, z) \;=\; \frac{1}{T}\int_{-\infty}^{\infty} \mathrm{d}z |\psi_{\mathrm{in}}(x = y = 0, z, t < 0)|^2 \;. \tag{3.92}$$

We use a wave packet that is sufficiently broad that this flux is constant over the entire extent of the region with $V \neq 0$.

The detection rate is proportional to the probability to find the particle in the box shown in Fig. 3.14:

$$\frac{\mathrm{d}N_{\mathrm{det}}}{\mathrm{d}t} \;=\; \frac{1}{T}(\mathrm{d}\theta)^2 \int_0^{\infty} \mathrm{d}r\, r^2 |\psi_{\mathrm{sc}}(r, \theta, t \gg 0)|^2 \;. \tag{3.93}$$

Using (3.91), we find

$$\frac{\mathrm{d}\sigma}{\mathrm{d}\Omega} \;=\; \frac{\int \mathrm{d}r\, |\psi_{\mathrm{sc}}(r, \theta, t \gg 0)|^2 r^2}{\int \mathrm{d}z\, |\psi_{\mathrm{in}}(x = y = 0, z, t < 0|^2} \tag{3.94}$$

To calculate the differential cross-section we need only calculate ψ_{sc} for a given ψ_{in}. To do this, it is useful to express the wavefunction as a superposition of the energy eigenfunctions $\psi_E(\boldsymbol{r})$ satisfying the eigenvalue equation

$$-\frac{\hbar^2}{2m}\nabla^2 \psi_E(\boldsymbol{r}) + V(\boldsymbol{r}, t)\psi_E(\boldsymbol{r}) \;=\; E\psi_E(\boldsymbol{r}) \;. \tag{3.95}$$

For $V = 0$ the eigenfunctions are just the familiar plane waves, $\exp(\mathrm{i}\boldsymbol{p} \cdot \boldsymbol{r}/\hbar)$ and a superposition makes a wave packet of the form

$$\psi(\boldsymbol{r}, t) \;=\; \frac{1}{(2\pi)^{3/2}} \int \mathrm{d}^3k\, \phi(\boldsymbol{k})\, \mathrm{e}^{\mathrm{i}(\boldsymbol{k}\cdot\boldsymbol{r} - \omega(k)t)} \;, \tag{3.96}$$

where $\boldsymbol{k} = \boldsymbol{p}/\hbar$ and $\omega(k) = E(p)/\hbar$. With $V = V(r) \neq 0$, far from the target, $r \gg R$, the eigenfunctions are sums of plane waves and radial waves emanating from the target:

$$\psi(\boldsymbol{r}, t) \;=\; \frac{1}{(2\pi)^{3/2}} \int \mathrm{d}^3k\, \phi(\boldsymbol{k}) \left[\mathrm{e}^{\mathrm{i}\boldsymbol{k}\cdot\boldsymbol{r}} + \frac{f(\theta)}{r}\mathrm{e}^{\mathrm{i}kr}\right] \mathrm{e}^{-\mathrm{i}\omega(k)t} \;. \tag{3.97}$$

The first term in the integral represents the initial and transmitted wave packet and the second term is the scattered wave. (We will see that the second term integrates to zero for $t \ll 0$ so it does not contribute to the initial wave packet.) The "scattering amplitude" $f(\theta)$ is a function of the angle between the momentum $\boldsymbol{p}$ and the position vector $\boldsymbol{r}$:

$$\cos\theta(\boldsymbol{k},\boldsymbol{r}) \;=\; \frac{\boldsymbol{k}\cdot\boldsymbol{r}}{|\boldsymbol{k}||\boldsymbol{r}|}. \tag{3.98}$$

Since $f(\theta)$ has the dimensions of length, we can anticipate that

$$\frac{\mathrm{d}\sigma}{\mathrm{d}\Omega} \;=\; |f(\theta)|^2\,. \tag{3.99}$$

To describe a particle impinging on the target along the z direction we take $\phi(\boldsymbol{k})$ to be strongly peaked at $\boldsymbol{k}_0 = (k_x = 0, k_y = 0, k_z = k_0 = p_0/\hbar)$. Therefore only the values of $\boldsymbol{k}$ near $\boldsymbol{k}_0$ will contribute. We therefore expand $\omega(k)$

$$\begin{aligned}\hbar\omega(k) &= E(p_0) + \boldsymbol{\nabla}E(\boldsymbol{p})\cdot(\boldsymbol{p}-\boldsymbol{p}_0) \;+\ldots \\ &= E(p_0) + v_0(p_z - p_0) + \ldots\,,\end{aligned} \tag{3.100}$$

where $\boldsymbol{v}_0$ is the group velocity. For a wave packet representing a massive particle, the group velocity is the classical velocity $v_0 = p_0/m$. Keeping only the first two terms in the expansion, the first term of (3.97) is

$$\psi_{\mathrm{in}}(\boldsymbol{r},t) \;=\; \frac{1}{(2\pi)^{3/2}}\mathrm{e}^{\mathrm{i}(k_0 z-\omega_0 t)}\psi_{\mathrm{env}}(\boldsymbol{r}-\boldsymbol{v}_0 t)\,, \tag{3.101}$$

where the "envelope" function is

$$\psi_{\mathrm{env}}(\boldsymbol{r}-\boldsymbol{v}_0 t) \;=\; \int \mathrm{d}^3k\,\phi(\boldsymbol{k})\,\mathrm{e}^{\mathrm{i}(\boldsymbol{k}-\boldsymbol{k}_0)\cdot(\boldsymbol{r}-\boldsymbol{v}_0 t)}\,. \tag{3.102}$$

We see that ψ_{in} is the product of a plane wave and an envelope that is a function only of $\boldsymbol{r}-\boldsymbol{v}_0 t$, i.e. the envelope moves with the group velocity. For example, if $\phi(\boldsymbol{k})$ is a real Gaussian function peaked at $\boldsymbol{k}-\boldsymbol{k}_0 = 0$, then the envelope will be a Gaussian peaked at $\boldsymbol{r}-\boldsymbol{v}_0 t = 0$, i.e. at $\boldsymbol{r} = \boldsymbol{v}_0 t$, with the variances of the Gaussians satisfying the Heisenberg uncertainty relations $\sigma_x\sigma_{p_x} = \sigma_y\sigma_{p_y} = \sigma_z\sigma_{p_z} \sim \hbar$. Including higher-order terms in the expansion (3.100) leads to spreading of the wave packet at large times.

The scattered wavefunction has a similar structure:

$$\psi_{\mathrm{sc}}(r,\theta,t) \;=\; \frac{f(\theta)}{r}\mathrm{e}^{\mathrm{i}(k_0 r-\omega_0 t)}\int \mathrm{d}^3k\,\phi(\boldsymbol{k})\,\mathrm{e}^{\mathrm{i}(k_z-k_0)(r-v_0 t)} \tag{3.103}$$

where we have dropped a factor $\exp(\mathrm{i}(k_x^2+k_y^2)r/k_0)$ which is near unity for a sufficiently wide wave packet. We have also taken $f(\theta)$ out of the integral since $\phi(\boldsymbol{k})$ is strongly peaked around $\boldsymbol{k}_0$ and therefore (3.98) is well approximated by

$$\cos\theta \;\sim\; \frac{\boldsymbol{k}_0\cdot\boldsymbol{r}}{|\boldsymbol{k}_0||\boldsymbol{r}|}\;. \tag{3.104}$$

Comparing (3.102) and (3.103), we see that

$$|\psi_{\rm sc}(r-v_0t,\theta,t)|^2 \;=\; \frac{|f(\theta)|^2}{r^2}|\psi_{\rm in}(x=y=0,z=r-v_0t)|^2\;. \tag{3.105}$$

This tells us the scattered wavefunction is simply a replica of $\psi_{\rm in}$ that is scaled down by a factor $f(\theta)/r$. Note also that (3.105) implies that the scattered wave vanishes for $t \ll 0$ since it is proportional to the incident wave at $(t \ll 0, z \gg 0)$ which vanishes.

Substituting (3.105) into (3.94) we find the required identification of the differential scattering cross-section and the square of the scattering amplitude (3.99).

We now need to find the relation between $f(\theta)$ and the potential $V(r)$. This is easy to do if the potential is sufficiently weak that the wave packet is only slightly perturbed as it passes through the potential. We rewrite the eigenvalue equation (3.95) as

$$(\nabla^2-k^2)\psi_k(\boldsymbol{r}) \;=\; 2mV(r)\psi_k(\boldsymbol{r})/\hbar^2 \tag{3.106}$$

where $k=\sqrt{2mE}/\hbar$. We will look for solutions of the form

$$\psi_k \;=\; \mathrm{e}^{\mathrm{i}kz} \;+\; \psi_{k\,\rm sc}\;, \tag{3.107}$$

where the first term is a solution of the eigenvalue equation with $V=0$ and the second term is a particular solution to the equation with $V\neq 0$.

Since the effect of the potential is assumed to be small, it should be a good approximation to replace the wavefunction of the right-hand side of (3.106) with the incident plane wave:

$$(\nabla^2-k^2)\psi_k(\boldsymbol{r}) \;=\; 4\pi S(\boldsymbol{r})\;, \tag{3.108}$$

where

$$S(\boldsymbol{r}) = \frac{2mV(r)\exp(\mathrm{i}\boldsymbol{k}\cdot\boldsymbol{r})}{4\pi\hbar}\;. \tag{3.109}$$

For $k=0$ this is the Poisson equation of electrostatics with the electrostatic potential replaced by $\psi_k(\boldsymbol{r})$ and the charge density replaced by $S(\boldsymbol{r})$. The solution is well-known:

$$\psi_{k\,\mathrm{sc}}(\boldsymbol{r}) \;=\; \frac{1}{4\pi}\int \mathrm{d}^3r'\frac{1}{|\boldsymbol{r}-\boldsymbol{r}'|}S(\boldsymbol{r}') \qquad (k=0)\;. \tag{3.110}$$

For $k \neq 0$, the solution is only slightly more complicated:

$$\psi_{k\,\mathrm{sc}}(\boldsymbol{r}) \;=\; \frac{1}{4\pi}\int \mathrm{d}^3r'\frac{\exp(\mathrm{i}k|\boldsymbol{r}-\boldsymbol{r}'|)}{|\boldsymbol{r}-\boldsymbol{r}'|}S(\boldsymbol{r}')\;. \tag{3.111}$$

This formula has a simple physical interpretation: the scattered wave is a sum of spherical waves generated at each point $\boldsymbol{r}'$ in the potential well and having an amplitude proportional to $S(\boldsymbol{r}') \propto V(\boldsymbol{r}')$.

Equation (3.111) can be written as

$$\psi_{k\,\mathrm{sc}}(\boldsymbol{r}) \;=\; \frac{2m}{4\pi\hbar^2}\int \mathrm{d}^3r'\frac{\exp(\mathrm{i}k|\boldsymbol{r}-\boldsymbol{r}'|)\exp(\mathrm{i}kz')}{|\boldsymbol{r}-\boldsymbol{r}'|}V(r)\;. \tag{3.112}$$

We are interested in ψ_{sc} far from the scattering center in which case we can approximate $\boldsymbol{r}' = 0$ (in the denominator) and $|\boldsymbol{r}-\boldsymbol{r}'| \sim r - \boldsymbol{r}\cdot\boldsymbol{r}'/r$ (in the numerator). A particle observed at $\boldsymbol{r}$ will be interpreted as having a momentum $\boldsymbol{p}' = p_0\boldsymbol{r}/r$ implying $|\boldsymbol{r}-\boldsymbol{r}'| \sim r - \boldsymbol{k}'\cdot\boldsymbol{r}'/k_0$ so the scattered wavefunction is

$$\psi_k(\boldsymbol{r}) \;=\; \frac{2m\mathrm{e}^{\mathrm{i}kr}}{4\pi r}\int \mathrm{d}^3r'V(r')\exp(\mathrm{i}\boldsymbol{q}\cdot\boldsymbol{r}'/\hbar)\;, \tag{3.113}$$

where $\boldsymbol{q} = \boldsymbol{p}-\boldsymbol{p}'$ is the momentum transfer of magnitude $|\boldsymbol{q}|^2 = 2p_0^2(1-\cos\theta)$. We see that the scattered wave is proportional to the Fourier transform of the potential.

$$\tilde{V}(\boldsymbol{q}) = \int \mathrm{e}^{\mathrm{i}\boldsymbol{q}\cdot\boldsymbol{r}/\hbar}V(\boldsymbol{r})\mathrm{d}^3\boldsymbol{r}\;. \tag{3.114}$$

The differential cross section is then

$$\frac{\mathrm{d}\sigma}{\mathrm{d}\Omega} = \frac{m^2}{4\pi^2\hbar^4}|\tilde{V}(\boldsymbol{p}-\boldsymbol{p}')|^2 \tag{3.115}$$

as found in the previous section.

Equation, (3.115) tells us that the cross-section takes an especially simple form if $\boldsymbol{q} = 0$

$$\frac{\mathrm{d}\sigma}{\mathrm{d}\Omega}(\boldsymbol{q}=0) \;=\; \frac{m^2}{4\pi^2\hbar^4}\left|\left(\int V(r)\mathrm{d}^3r\right)\right|^2\;. \tag{3.116}$$

Since $\boldsymbol{q}^2 = 2p^2(1-\cos\theta)$, this condition is met either in the forward direction, $\theta = 0$, or in the low-energy limit where the de Broglie wavelength is much greater than the range of the potential, $\hbar/p \gg R$. For $\boldsymbol{q}^2 \neq 0$, the exponential in the integrand is an oscillating function of $\boldsymbol{r}'$ so the integral is suppressed.

This can be intuitively understood by saying that far from the region where $V \neq 0$, the spherical waves generated at different positions are not entirely in phase and therefore partially cancel. As seen in (3.112) and in Fig. 3.15, only for $\theta = 0$ or for $\hbar/p \gg R$ is the phase independent of $\boldsymbol{r}'$ so the spherical waves are entirely in phase at the observer's position $\boldsymbol{r}$.

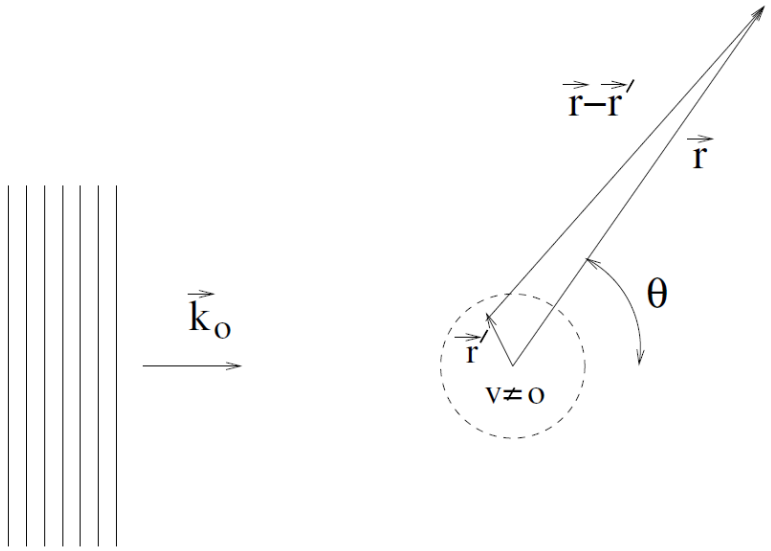

Fig. 3.16. A wave packet of central momentum $\boldsymbol{p}_0 = \hbar \boldsymbol{k}_0$ that impinges upon a region with $V(r) \neq 0$. The scattered wave packet at $\boldsymbol{r}$ is the superposition of spherical waves generated at each point $\boldsymbol{r}'$. A particle observed at $\boldsymbol{r}$ will be interpreted as having a momentum $\boldsymbol{p}' = p_0 \boldsymbol{r}/r$ implying a momentum transfer squared of $|\boldsymbol{q}|^2 = |\boldsymbol{p}' - \boldsymbol{p}|^2 = 2p_0^2(1 - \cos\theta)$.

The suppression of the cross-section for $\theta \neq 0$ because of destructive interference is quite different from the classical case. Here, the large angle cross-section is suppressed simply because the particle trajectory must pass near the center of the potential in order to produce a wide-angle scatter.

While the decline of the cross-section with increasing scattering angle has different origins in quantum and classical mechanics, we saw previously that the classical and quantum calculations may give identical answers as long as $\boldsymbol{q}^2 \neq 0$. In fact, what distinguishes quantum scattering from classical scattering is that in quantum scattering the cross-section must be isotropic for $qR \ll 1$. This condition is met at all scattering angles if the de Broglie wavelength of the incident particle is much greater than the range R of the potential. This is equivalent to the condition

$$\frac{p^2}{2m} < \frac{(\hbar c)^2}{8R^2 mc^2} = 5\,\mathrm{MeV}\,\frac{1\,\mathrm{GeV}}{mc^2}\left(\frac{1\,\mathrm{fm}}{R}\right)^2 . \tag{3.117}$$

For incident energies below this limit, the scattering must be isotropic. For incident energies above this limit, the scattering will still be isotropic at small angles:

$$\theta < \frac{\hbar c}{\sqrt{2(p^2/2m)mc^2}R} = 2\left(\frac{5\,\mathrm{MeV}}{p^2/2m}\right)^{1/2}\left(\frac{1\,\mathrm{GeV}}{mc^2}\right)^{1/2}\frac{1\,\mathrm{fm}}{R}\,, \quad (3.118)$$

where we have taken the small-angle limit $(1-\cos\theta) = \theta^2/2$. For angles larger than this values, the cross-section decreases, as seen in Fig. 3.6.

Particle-particle scattering

We now return to the treatment of scattering using time-dependent perturbation theory as in Sect. 3.3.2. In this section, we complicate slightly the scattering problem by taking into account the recoil of the target particle. The immediate result will be that the translation invariance of the Hamiltonian enforces momentum conservation, a fact that was ignored in fixed-potential scattering.

Scattering of two free particles

We consider now the scattering to two particles, 1 and 2, with initial momenta $\boldsymbol{p}_1$ and $\boldsymbol{p}_2$, and final momenta $\boldsymbol{p}'_1$ and $\boldsymbol{p}'_2$. We take the potential energy to be $V(\boldsymbol{r}_1 - \boldsymbol{r}_2)$, i.e. a function only of the *relative coordinates* of the two particles. The conservation of momentum will be a consequence of the assumption that the interaction potential $V(\boldsymbol{r}_1 - \boldsymbol{r}_2)$ is translation invariant.

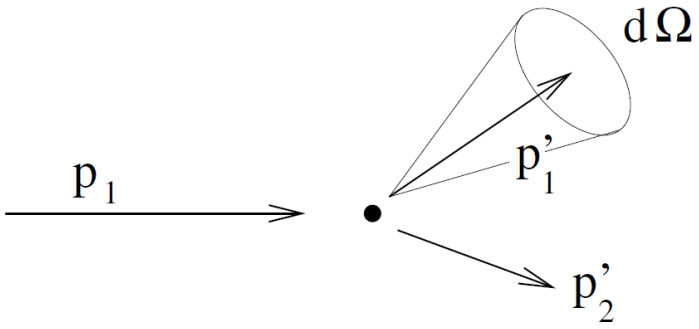

Fig. 3.17. Scattering of two particles with recoil.

The treatment of this problem follows the treatment of scattering on fixed potential starting with the transition rate given by (3.56). The initial and final state wavefunctions are now

$$\psi_i(\boldsymbol{r_1}, \boldsymbol{r_2}) = \frac{\mathrm{e}^{\mathrm{i}\boldsymbol{p}_1\cdot\boldsymbol{r_1}}}{L^{3/2}}\frac{\mathrm{e}^{\mathrm{i}\boldsymbol{p}_2\cdot\boldsymbol{r_2}}}{L^{3/2}} \qquad \psi_f(\boldsymbol{r_1}, \boldsymbol{r_2}) = \frac{\mathrm{e}^{\mathrm{i}\boldsymbol{p}'_1\cdot\boldsymbol{r_1}}}{L^{3/2}}\frac{\mathrm{e}^{\mathrm{i}\boldsymbol{p}'_2\cdot\boldsymbol{r_2}}}{L^{3/2}}\,. \quad (3.119)$$

The matrix element between initial and final states is

$$\langle f|V|i\rangle = \frac{1}{L^6}\int \mathrm{e}^{\mathrm{i}(\boldsymbol{p}_1-\boldsymbol{p}'_1)\cdot\boldsymbol{r}_1/\hbar}\mathrm{e}^{\mathrm{i}(\boldsymbol{p}_2-\boldsymbol{p}'_2)\cdot\boldsymbol{r}_2/\hbar}V(\boldsymbol{r}_1-\boldsymbol{r}_2)\mathrm{d}^3\boldsymbol{r}_1\mathrm{d}^3\boldsymbol{r}_2$$

$$= \frac{1}{L^6} \int \mathrm{e}^{\mathrm{i}(\boldsymbol{p}_1 - \boldsymbol{p}_1') \cdot (\boldsymbol{r}_1 - \boldsymbol{r}_2)/\hbar} \mathrm{e}^{\mathrm{i}(\boldsymbol{p}_1 + \boldsymbol{p}_2 - \boldsymbol{p}_1' - \boldsymbol{p}_2') \cdot \boldsymbol{r}_2/\hbar} V(\boldsymbol{r}_1 - \boldsymbol{r}_2) \mathrm{d}^3\boldsymbol{r}_1 \mathrm{d}^3\boldsymbol{r}_2 \ .$$

Replacing the integration variable $\boldsymbol{r}_1$ by $\boldsymbol{r} = \boldsymbol{r}_1 - \boldsymbol{r}_2$, we find

$$\langle f|V|i\rangle \ = \ \frac{\tilde{V}(\boldsymbol{p}_1 - \boldsymbol{p}_1')}{L^6} (2\pi\hbar)^3 \Delta_L^3(\boldsymbol{p}_1 + \boldsymbol{p}_2 - \boldsymbol{p}_1' - \boldsymbol{p}_2') \ , \tag{3.120}$$

where

$$\Delta_L^3(\boldsymbol{p}) \ = \ \prod_{i=x,y,z} \left(\frac{1}{\pi} \frac{\sin p_i L/2\hbar}{p_i} \right) \tag{3.121}$$

is a limiting form of the three-dimensional delta function (see Appendix C.0.2). The matrix element is the product of the Fourier transform of the potential introduced previously and an oscillating function (3.121) whose role, when squared, is to force momentum conservation:

$$[\Delta_L^3(\boldsymbol{p})]^2 \ = \ \frac{L^3 \delta^3(\boldsymbol{p})}{(2\pi\hbar)^3} \ . \tag{3.122}$$

Substituting into (3.56), the transition rate to the final state is

$$\lambda_{i\to f} \ = \ \frac{2\pi}{\hbar} \frac{|\tilde{V}(\boldsymbol{p}_1 - \boldsymbol{p}_1')|^2}{L^{12}} \delta(E_f - E_i) L^3 (2\pi\hbar)^3 \delta^3(\boldsymbol{p}_1 + \boldsymbol{p}_2 - \boldsymbol{p}_1' - \boldsymbol{p}_2') \ .$$

The number of states within the momentum volume $\mathrm{d}^3\boldsymbol{p}_1' \mathrm{d}^3\boldsymbol{p}_2'$ is

$$\mathrm{d}N \ = \ \frac{L^3 \mathrm{d}^3\boldsymbol{p}_1'}{(2\pi\hbar)^3} \frac{L^3 \mathrm{d}^3\boldsymbol{p}_2'}{(2\pi\hbar)^3} \ . \tag{3.123}$$

The total transition rate into these states is then

$$\lambda(\mathrm{d}^3\boldsymbol{p}_1', \mathrm{d}^3\boldsymbol{p}_2') \ = \tag{3.124}$$

$$\left(\frac{L}{2\pi\hbar} \right)^3 \mathrm{d}^3\boldsymbol{p}_1' \mathrm{d}^3\boldsymbol{p}_2' \frac{2\pi}{\hbar} \frac{|\tilde{V}(\boldsymbol{p}_1 - \boldsymbol{p}_1')|^2}{L^6} \delta(E' - E) \delta^3(\boldsymbol{p}_1 + \boldsymbol{p}_2 - \boldsymbol{p}_1' - \boldsymbol{p}_2') \ .$$

Integrating over $\mathrm{d}^3\boldsymbol{p}_2'$, we find the transition rate

$$\lambda(\mathrm{d}^3\boldsymbol{p}_1') \ = \tag{3.125}$$

$$\left(\frac{L}{2\pi\hbar} \right)^3 \mathrm{d}^3\boldsymbol{p}_1' \frac{2\pi}{\hbar} \frac{|\tilde{V}(\boldsymbol{p}_1 - \boldsymbol{p}_1')|^2}{L^6} \delta(E_1' + E_2' - E_1 - E_2) \ ,$$

where $E_2' = E_2(\boldsymbol{p}_1 + \boldsymbol{p}_2 - \boldsymbol{p}_1')$ is determined by momentum conservation.

This is the same transition rate as in the fixed potential case (3.68) except that the energy-conservation delta function now includes the effect of nuclear recoil. If the nuclear recoil is negligible, the reaction rate is identical to that calculated for a fixed potential. In particular, for a heavy target at rest, we have $E_2 = m_2c^2$ and $E_2' = m_2c^2 + (p_2')^2/2m_2$ and

$$\lambda(\mathrm{d}^3\boldsymbol{p}_1') \;=\; \left(\frac{L}{2\pi\hbar}\right)^3 \mathrm{d}^3\boldsymbol{p}_1' \frac{2\pi}{\hbar} \frac{|\tilde{V}(\boldsymbol{p_1} - \boldsymbol{p_1'})|^2}{L^6} \delta(E_1' - E_1 + (p_2')^2/2m_2) \;,$$

which reduces to the fixed potential result when $m_2 \to \infty$.

Another interesting limit is the collision of two ultra-relativistic particles. We treat the problem in the center-of-mass so that $E_1 = E_2 = E_{\mathrm{cm}}/2$. The transition rate is

$$\lambda(\mathrm{d}^3\boldsymbol{p}_1') \;=\; \left(\frac{L}{2\pi\hbar}\right)^3 \mathrm{d}^3\boldsymbol{p}_1' \frac{2\pi}{\hbar} \frac{|\tilde{V}(\boldsymbol{p_1} - \boldsymbol{p_1'})|^2}{L^6} \delta(2E_1' - 2E_1) \;, \tag{3.126}$$

or

$$\lambda(\mathrm{d}\Omega, \mathrm{d}E_1') \;= \tag{3.127}$$

$$\frac{2c}{L^3}\left(\frac{1}{2\pi\hbar}\right)^3 \mathrm{d}\Omega p_1' E_1' \mathrm{d}E_1' \frac{\pi}{\hbar c} |\tilde{V}(\boldsymbol{p_1} - \boldsymbol{p_1'})|^2 \delta(2E_1' - 2E_1) \;.$$

Dividing by the factor $2c/L^3$ gives the cross-section (where L cancels off identically).

A simple example is high-energy neutrino–electron elastic scattering in which case $\tilde{V} \propto G_{\mathrm{F}}$. This gives isotropic scattering in the center-of-mass

$$\frac{\mathrm{d}\sigma}{\mathrm{d}\Omega} \;\propto\; \frac{G_{\mathrm{F}}^2 E_{\mathrm{cm}}^2}{4\pi^2} \;, \tag{3.128}$$

with a total cross-section of

$$\sigma \;\propto\; \frac{G_{\mathrm{F}}^2 E_{\mathrm{cm}}^2}{\pi} \;. \tag{3.129}$$

The correct numerical factors are given in Table 3.1.

By taking into account the recoil of the target, we have introduced that added constraint of momentum conservation into the cross-section. Since momentum conservation is the result of the translation invariance of the Hamiltonian, we can anticipate that it will hold in more general reactions between two (or more) free particles. Consider a reaction

$$a_1 + a_2 \to b_1 + b_2 + \ldots + b_n \;. \tag{3.130}$$

The initial momenta are $\boldsymbol{p}_1$ and $\boldsymbol{p}_2$ with $\boldsymbol{p} = \boldsymbol{p}_1 + \boldsymbol{p}_2$ being the total momentum and $E = E_1 + E_2$ the total energy. The final state momenta and energies are $\boldsymbol{q}_i,\ i = 1, \ldots, n$ and E'_i.

We can anticipate that the cross-section will be of the form

$$d\sigma = \frac{2\pi}{\hbar v_0} G(\boldsymbol{p}_1, \boldsymbol{p}_2; \boldsymbol{q}_1, \ldots, \boldsymbol{q}_n)(2\pi\hbar)^3$$

$$\times\, \delta(\boldsymbol{p} - \Sigma \boldsymbol{q}_i)\delta(E - \Sigma E'_i)\frac{\mathrm{d}^3\boldsymbol{q}_1}{(2\pi\hbar)^3} \cdots \frac{\mathrm{d}^3\boldsymbol{q}_n}{(2\pi\hbar)^3}\ , \qquad (3.131)$$

where G is the square of the relevant transition amplitude. This expression only has meaning after we integrate it over four independent variables (for instance one momentum and one energy) in order to remove the delta functions coming from the conservation of energy and momentum.

Finally, we note that, in general, the relative velocity v_0 of the initial particles is

$$v_0 = \left((\boldsymbol{v}_1 - \boldsymbol{v}_2)^2 - (\boldsymbol{v}_1 \wedge \boldsymbol{v}_2)^2/c^2\right)^{1/2} \qquad (3.132)$$

This expression must be used if the initial particles are not collinear.

u ∧ v means the wedge product of any multivectors u and v.

$u \wedge v = *(\mathrm{u} \times \mathrm{v})$ if $u, v \in \mathrm{R}^3$